8-2018

Proposed ASTM Standard for the Stokoe-type Resonant Column Torsional Shear Device

Anh Tuan Tran
University of Arkansas, Fayetteville

Proposed ASTM Standard for the Stokoe-type Resonant Column Torsional Shear Device

A thesis submitted in partial fulfilment
of the requirements for the degree of
Master of Science in Civil Engineering

by

Anh Tuan Tran
Water Resource University
Bachelor of Science in Civil Engineering, 2015

August 2018
University of Arkansas

This thesis is approved for recommendation to the Graduate Council

_____
Richard A. Coffman, Ph.D., P.E., P.L.S.
Thesis Director

_____
Michelle L. Bernhardt-Barry, Ph.D., P.E.
Committee Member

_____
Clinton M. Wood, Ph.D., P.E.
Committee Member

ABSTRACT

Resonant Column Torsional Shear (RCTS) testing has become one of the most commonly used methods for determining laboratory soil stiffness and soil damping. The RCTS test has been accepted and is commonly utilized during the permitting of new nuclear facilities. However, there is still no available public standard for performing RCTS tests using the Stokoe-type device. Therefore, an ASTM standard for calibration and performance of RCTS tests using the Stokoe-type RCTS device is presented herein. Data collected using the Stokoe-type RCTS devices at the University of Arkansas (UofA) and at the Norwegian Geotechnical Institute (NGI) also aided in the development of this standard.

By following the proposed standard to calibrate the RCTS Stokoe-type device, the mass polar moment of inertia value, J_o, for the UofA drive plates were found to be similar but smaller than to J_o values found by other authors. The proximeter calibration factor, K_P, was determined to be valid because the obtained results were consistent for the linear calibration method and for the rotational calibration method (0.0028 rad/V). The torque calibration factor, K_T, was also determined to be valid with the obtained value of 0.1347 N·m/V.

To validate the proposed ASTM standard, RCTS tests following the standard were performed on Ottawa Sand specimens using the Stokoe-type devices at the UofA. The obtained modulus reduction curves and damping curves were compared with curves developed at the University of Texas. The UofA obtained modulus reduction curves were found to plot at higher values than the Texas curves, but both curves followed the same trend. The UofA damping curves compared well with the Texas curves at shear strain levels less than 10^{-2} percent, but it was above the Texas obtained curves at shear strain levels greater than 10^{-2} percent.

Shear wave velocity values for the Ottawa Sand specimens from the RCTS tests were also compared with results obtained from bender element test performed on similar specimens at the

same confining pressure. A only five (5) percent difference in shear wave velocities was observed between the bender element obtained values (178 m/s) and the resonant column obtained values (187 m/s).

ACKNOWLEDGMENTS

This masters thesis was funded by the Vietnam Education Foundation (VEF) Fellowship. Thanks are extended to VEF and to all of the people who supported me during my academic journey. Specifically, thanks are provided to my family who respected my decision to obtain my masters degree, including my parents Thanh Tran and Van Dang, and my younger sister Trang Tran. Appreciation is also shown to my advisor, Dr. Richard Coffman. Although I have only worked with Dr. Coffman for almost two years, I can see his passion and dedication to Geotechnical Engineering and to his students. Dr. Coffman is a great teacher and a role model for me to follow. I am also grateful to my committee members and other teachers I have had during my study at the University of Arkansas (Dr. Michelle L. Bernhardt-Barry, Dr. Clinton Wood, Dr. Panneer Selvam and Dr. Eric Fernstrom). Appreciation is expressed to my colleagues and Geo-Institute friends who helped me and travelled with me along the way: Johnathan Blanchard, Elvis Ishimwe, Nabeel Mahmood, Anibal Santos, Sean Salazar, Nichole Elliott, Mateo Lopez, Nathan Parnell, Ashraf Himel, Salman Rahimi, Folaseye Coker, Claire Stewart, Esteban Pinzon and Gregory Thomas. Finally, thanks are extended to all the members of the Badminton Club, Vietnamese Student Association, and International Culture Team Band who made me feel like I was at home while at the University of Arkansas.

TABLE OF CONTENTS

LIST OF FIGURES

LIST OF TABLES

CHAPTER 1: INTRODUCTION

1.1. Background

Any engineered structure subjected to dynamic loading must be designed to account for the effects of the dynamic loads on the soils beneath the structure (Hwang, 1997). Dynamic loading can result from an earthquake, blasting, machinery, vehicular traffic (especially railroad or heavy automobile), pile driving, wave forces, construction or other types of live load. In geotechnical engineering, the two properties that are most frequently utilized to design, for soil response to dynamic loading, include 1) the shear modulus and 2) the material damping ratio (Kramer, 2014). The shear modulus corresponds to the soil stiffness and the material damping represents the energy dissipation parameter for a given soil.

There are two different approaches that are commonly utilized to measure soil dynamic properties. The first approach is field testing (in-situ seismic measurement) and the second approach is laboratory testing (Scheer, 1992). As per Kim (1991), field testing can include invasive tests, like crosshole, downhole, and seismic cone penetration tests or non-invasive tests like Spectral Analysis of Surface Waves (SASW) or Multichannel Analysis of Spectral Waves (MASW) testing. Field tests rely on generating stress waves (primary, secondary, or Rayleigh waves) at the ground surface and then analyzing the wave propagation through the soil layers to determine the dynamic soil properties. The main advantage of field testing methods is that tests are performed in situ, which minimizes the effects of sample disturbance and minimizes the risk of obtaining non-representative specimens for associated laboratory testing. However, the effects of stress state, strain amplitude, excitation frequency and number of loading cycles cannot be investigated when utilizing field tests (Hwang, 1997). In addition, only small amounts of strain are induced during field measurements, which limit the measurements of shear modulus to strain

values of less than 10^{-3} percent (Kim, 1991). The typical range of strains associated with different field measurements and laboratory measurements is presented in Figure 1.1.

Laboratory tests are commonly utilized to overcome the small-strain limitations of field measurements. Common laboratory tests include: resonant column, piezoelectric bender element, torsional shear, combined resonant column and torsional shear (RCTS), cyclic triaxial, and cyclic simple shear tests. The limitations of the laboratory tests include sample disturbance and the development of unrepresentative samples. A better sampling method and collection of more soil specimens may help to minimize these aforementioned limitations.

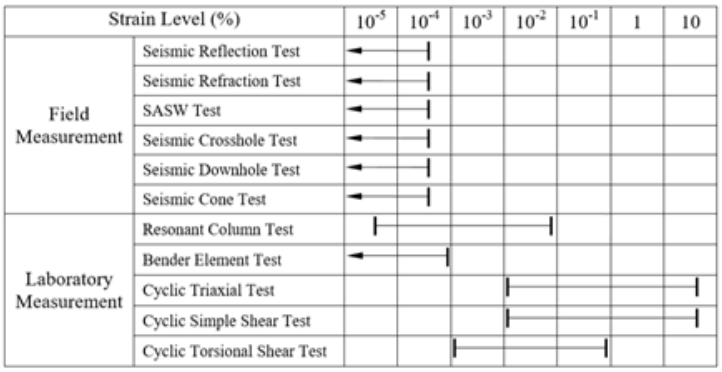

Figure 1.1. Typical strain levels associated with different dynamic soil techniques (from Sasanakul, 2005).

1.2. Introduction about RCTS tests at the University of Arkansas

In July 2011, the University of Arkansas (UofA) received two Stokoe-type RCTS devices that were previously owned by the South Texas Nuclear Project. The South Texas Nuclear Plant purchased the devices and provided the devices to Fugro Consultants to complete RCTS testing for a permit application for the proposed Unit 3 and Unit 4 expansion at the South Texas Nuclear Project in Palacios, Texas. The two RCTS devices, data acquisition systems, operating software, and calibration specimens were fabricated and assembled by the Trautwein Soil Testing Equipment Company in Houston, Texas.

Several advantages related to RCTS test have been identified in the literature. For example, RCTS tests are less susceptible to soil specimen and equipment variability because both the RC (dynamic test) and the TS (cyclic test) can be performed on the same specimen. Additionally, the RCTS device enables samples to be tested over a wide range of strains (from 10^{-5} percent to 10^{-1} percent) when compared to other dynamic testing techniques. The RCTS device can also be used to test soil at a wide range of frequencies. Specifically, the RCTS device can be used to test from 10-400 Hz during RC testing or from 0.01-10 Hz during TS testing; therefore, the effect of frequency on deformational characteristics can be effectively investigated (Kim, 1991). Finally, the RCTS test is performed in a pressurized cell, allowing for different confining stresses to be applied to the soil specimen to simulate field conditions.

The RCTS device also has several disadvantages. These disadvantages include: 1) the method is complicated and requires accurate calibration procedures, 2) extra damping is associated with the equipment, and 3) non-uniform levels of stress and strain are developed within the sample during testing. Ultimately, the testing method that is selected for a particular project should be carefully considered and selected based on the specific parameters required and the goals of the project.

1.3. Objective

Two common types of Resonant Column (RC) devices currently exist. These device types include the Hardin and Drnevich-type device and the Stokoe-type device. Accurate resonant column testing is dependent on correctly calibrating the resonant column device. Calibration of the resonant column device is a complicated process. Recently, an ASTM standard was developed for the Hardin and Drnevich-type device (ASTM D4015, 2015). However, there is

currently no publicly published standardized testing procedure or calibration procedure for the Stokoe-type device.

Because 1) the Stokoe-type RCTS test has become the industry standard and 2) the Stokoe-type RCTS device is the type of device that is utilized at the University of Arkansas, the proposed standard contained herein (Chapter 3) will be primarily focused on the Stokoe-type RCTS device. However, the same methods utilized for the Stokoe-type RCTS device could also be applied to other types of RCTS devices, as well as resonate column tests and cyclic torsional shear tests in general.

The work performed for this thesis was completed to fulfill the objective of providing a new ASTM standard to calibrate and perform dynamic tests using Stokoe-type RCTS devices. Verification tests were performed on Ottawa Sand, using the calibrated RCTS devices at the UofA, to validate the proposed ASTM Standard. Specifically, data collected using the RCTS devices at the UofA aided in the development of the proposed ASTM standard.

1.4. Organization

This thesis is divided into six chapters. A literature review that includes the latest development of the two resonant column designs (the Stokoe-type device and the Hardin and Drnevich-type device) is included as Chapter 2. The literature review also includes a description of current available ASTM standards for shear modulus and damping ratio calculation using the Resonant Column, Cyclic Triaxial, and Torsional Ring Shear devices (Chapter 2). The proposed standard test method for the determination of modulus and damping of soils by using the Stokoe-type RCTS device is presented in Chapter 3. The methods used for, and the results obtained from, the calibration procedure are provided in Chapter 4. The results and discussion related to the RCTS verification tests that were performed on Ottawa Sand using the proposed standard are

presented in Chapter 5. A summary of the main findings and recommendations for future work are presented in Chapter 6.

CHAPTER 2: LITERATURE REVIEW

2.1. Chapter Overview

A review of relevant literature is contained within this chapter. The advancement of the Resonant Column test is presented in Section 2.2. The development of the Stokoe-type RCTS apparatus is presented in Section 2.3. Finally, a review of relevant ASTM test standards such as the Resonant Column standard, Cyclic Triaxial standard, and Torsional Ring Shear standard are presented in Section 2.4.

2.2. Advancement of the Resonant Column Test

The resonant column device was originally used by Japanese engineers (Ishimoto and Iida, 1936; and Iida, 1938 and 1940) to investigate the effect of soil parameters (length, porosity and moisture content) on the propagation velocity of elastic waves in sand (Kim, 1991). Over the past 50 years, most of the advancement in combatting various disadvantages and promoting improvements to the RC testing method have come from Dr. Richart, Dr. Hardin, Dr. Drnevich, Dr. Stokoe, or from students studying under these professors (Hardin and Richart 1963, Hardin 1965, Drnevich 1967, Stokoe 1972). The work of Dr. Richart and Dr. Hardin originally focused on the determination of the shear modulus and damping ratio by applying torsional excitation to a soil specimen. In 1965, Dr. Hardin developed a fixed-free torsional resonant column device named the "Hardin device" which was capable of applying the confining stress to a solid soil specimen (Ni, 1987). In 1967, Dr. Drnevich modified the "Hardin device" to 1) conduct the test on a hollow soil specimen to help to minimize the non-uniform stress/strain problem and to 2) enhance the shearing strain amplitude above 0.1 percent (Kim, 1991). During the late 1970, Dr. Stokoe and his students developed a new torsional resonant column, named the Stokoe-type Resonant Column Torsional Shear (RCTS) device. The RCTS device is unique because both the

resonant column test and the torsional shear test can be conducted on the same soil specimen when using the Stokoe-type RCTS device (Isenhower, 1979). Since the inception of the Stokoe-type RCTS device, it has become one of the most commonly used devices, in research and commercial settings, for determination of laboratory soil stiffness and damping. For example, the RCTS testing procedure is an accepted method that is commonly utilized for determining modulus and damping parameters of soils during the permitting of new nuclear facilities, as per the U.S. Nuclear Regulatory Commission Regulation Guide 1.208 Guidelines (2007).

Of the two designs (the Hardin and Drnevich-type or the Stokoe-type), information is more widely available for the Stokoe-type device. For example, the Stokoe-type device has been the subject of several papers (Ni 1987, Kim 1991, Scheer 1992, Darendeli 2001, Menq 2003, Sasanakul 2005, Keene 2017 to name a few). Although the Stokoe-type device is more frequently used, there is no available standard testing procedure that exists for this device. A new standard testing procedure (ASTM D4015, 2015) does exist for the Hardin and Drnevich-type device.

2.3. Stokoe-type RCTS Device Developement

Most of the Stokoe-type RCTS device developments have been completed at The University of Texas over the past four decades. For example, Isenhower (1979), Allen (1982), Lodde (1982), Ni (1987), Kim (1991), Menq (2003) and Keene (2017) have all advanced the capability of the Stokoe-type RCTS device. Initially, Isenhower (1979) modified the fixed-free resonant column device to allow for performance of both the resonant column test and the torsional shear test on the same soil specimen. Allen (1982) modified both the top cap and base pedestal for a solid specimen so that a thin central wire, which was rigidly attached to the top cap and passed through the base pedestal, could be connected to a frictionless piston secured beneath the support

table to apply an additional vertical stress. With these modifications, the device was able to apply an anisotropic loading ($\sigma'_1 > \sigma'_2 = \sigma'_3$) to the solid specimen. Ni (1987) modified the top cap and the base pedestal to enable application of different levels of pressure between the inner and outer cell pressures on hollow specimens. With these modifications and by controlling 1) the axial loading, 2) the inner cell pressure and 3) the outer cell pressure independently, the true triaxial states of stress were applied to hollow specimens. Ni (1987) also developed a computer-aided testing system to control the test and to collect data automatically.

Kim (1991) enhanced the proximeter system and applied a low-pass filter to control ambient noise so that the shear modulus for the TS tests could be measured at shearing strain levels as low as 10^{-5} percent instead of 10^{-4} percent that was commonly measured by traditional dynamic testing using a fixed-free resonant column device. To be more specific, Kim (1991) replaced the existing proximeter system with a micro-proximeter system that had a resolution that was approximately ten times greater than the previous resolution to obtain a proper stress-strain hysteresis loops at small-strain amplitude levels. Kim (1991) also used a pair of proximeters so that the signals could be compared and averaged to assure that 1) pure torsion was generated in the soil specimens and that 2) bending motions were cancelled. Finally, Kim (1991) installed a vibration isolation table to isolate the RCTS equipment from ambient vibrations to further improve the small-strain measurements.

Menq (2003) developed a multi-mode device that was able to measure the dynamic properties of large-grained soils in multiple modes including shear, unconstrained compression, and constrained compression. Keene (2017) improved the RCTS testing device and data acquisition system to enhance a better range of shear strain measurement in the RCTS test and to alleviate the limitations of the traditional RCTS device. By improving the signal processing

techniques, the shear strain was able to be measured accurately in the range from 10^{-6} percent to 10^{-1} percent.

2.4. Relevant Standards

There are various laboratory testing methods that have been developed and used to determine the deformational properties of soils. In general, these laboratory tests can be categorized into two groups: one group is dynamic tests and other group is cyclic tests (Kim, 1991). Dynamic tests are based on wave propagation and resonance measurements at high frequency levels. There are two common types of dynamic tests 1) dynamic tests that use the piezoelectric bender element test method and 2) dynamic tests that use the resonant column test method. For piezoelectric bender element tests, shear wave velocity values are obtained by measuring the travel time of shear wave from the inception at the point of origin to collection at the detection sensor. The initial standard test procedure for bender elements can be found in Dyvik and Madshus (1986). The resonant column test is based on the theory of one-dimensional wave propagation, and the testing procedures have been standardized in ASTM D4015 (2015). The ASTM D4015 (2015) is for the Hardin and Drnevich-type fixed-base resonant column device. Additional details regarding the development of the ASTM D4015 (2015) Standard can be found in Ashlock et al. (2015).

For the new Hardin and Drnevich resonant column testing device that is described in ASTM D4015 (2015), the torque that is applied at the top of specimen is measured at the bottom of the specimen to eliminate issues of back electromotive force (emf). Back emf is commonly created in RCTS testing due to movement of the magnet in the coil. The movement induces an electromotive force opposing the driving motion (Sasanakul, 2010). Based on the work of

Sasankul (2010), knowledge of the back emf is needed to properly calibrate the Stokoe-type RCTS device.

Unlike dynamic tests, cyclic tests are performed at low frequency levels, typically below 10Hz, and the deformational properties of the specimen are obtained from the developed stress-strain loop. The deformational properties of the specimen are typically measured at different levels of 1) confinement, 2) cyclic loads, and 3) number of loading cycles. Several types of cyclic tests are performed in the laboratory. These tests included the cyclic triaxial test, the cyclic simple shear test, and the cyclic torsional shear test. Among these tests, the cyclic triaxial test is the most common test. The standard test methods for the cyclic triaxial test are found in ASTM D3999 (2011): Standard Test Methods for the Determination of the Modulus and Damping Properties of Soils Using the Cyclic Triaxial Device. Another version of the cyclic triaxial standard is found in ASTM 5311 (2013): Standard Test Method for Load Controlled Cyclic Triaxial Strength of Soil. The basic idea of the cyclic triaxial test is to apply either a cyclic axial deviator stress of fixed magnitude (load control) or cyclic axial deformation (stroke control) on a consolidated soil specimen under undrained conditions. The resulting axial strain and axial stress are measured and used to calculate either stress-dependent or stroke-dependent secant modulus and damping ratio values.

For cyclic torsional shear tests, the basic idea is to apply cyclic torsional shear stresses about the vertical axis of the specimen. Like the RCTS test, the cyclic torsional shear test has a problem with non-uniform stress distribution because the shear stresses increase from zero at the axis of rotation to a maximum value at the outside radius. To account for this non-uniform stress-strain problem, Chen and Stokoe (1979) recommend using an equivalent radius of 0.82 for shearing strain less than 10^{-3} percent and 0.79 for shearing strain values equal to 0.1 percent for

solid specimens. There is no standard test for the cyclic torsional shear test, but following the static ring shear method ASTM D7608 (2010): Standard Test Method for Torsional Ring Shear Test may help to generalize how to perform the cyclic torsional shear test.

CHAPTER 3: A PROPOSED STANDARD TEST METHOD FOR DETERMINATION OF MODULUS AND DAMPING OF SOILS USING THE STOKOE-TYPE RESONANT COLUMN AND TORSIONAL SHEAR (RCTS) APPARATUS

3.1. Scope

3.1.1. The purpose of the test is to determine shear modulus values and damping ratio values as a function of shear strain by combining the results from the resonant column (RC) test and the torsional shear (TS) test. Both RC and TS tests are conducted on the same cylindrical specimen of soil in an intact or remolded condition, so the amount of uncertainty related to different specimen preparation is eliminated. The RCTS test method can be considered as a nondestructive testing method because only small level of maximum shear strain (less than 1 percent) is applied to the soil specimen.

3.1.2. Values stated in SI units are to be regarded as standard. No other units of measurement are included in this standard.

3.1.3. This standard does not purport to address all of the safety concerns, if any, associated with its use. It is the responsibility of the user of this standard to establish appropriate safety and health practices and determine the applicability of regulatory limitations prior to use.

3.2. Referenced Documents

ASTM Standards:

D653 Terminology Relating to Soil, Rock, and Contained Fluids.

D1587 Standard Practice for Thin-Walled Tube Sampling of Fine-Grained Soils for Geotechnical Purposes.

D2216 Test Methods for Laboratory Determination of Water (Moisture) Content of Soil and Rock by Mass.

D3999 Standard Test Methods for the Determination of the Modulus and Damping Properties of Soil Using the Cyclic Triaxial Apparatus.

D4015 Standard Test Methods for Modulus and Damping of Soils by Fixed-Base Resonant Column Devices.

D4220 Standard Practices for Preserving and Transporting Soil Samples.

D4767 Test Method for Consolidated Undrained Triaxial Compression Test for Cohesive Soils.

D5311 Standard Test Method for Load Controlled Cyclic Triaxial Strength of Soil.

D7608 Standard Test Method for Torsional Ring Shear Test to Determine Drained Fully Softened Shear Strength and Nonlinear Strength Envelope of Cohesive Soils (Using Normally Consolidated Specimen) for Slopes with no Preexisting Shear Surfaces.

3.3. Terminology

Definitions of terms used in this method is referred to ASTM D653.

Definitions of terms specific to this standard:

Resonant frequency, f_r, [Hz] - is the frequency at which the response amplitude is maximum.

Half-power bandwidth method - a method based on measurement of the width of the frequency response curve near the resonant frequency to measure the damping of the soil during the RC test.

Free-vibration decay method - a method that uses the decay curve collected by shutting off the power during the RC test, after the soil specimen reaches first-mode resonance, to measure the damping of the soil during the RC test.

Maximum shear modulus, G_{max}, [MPa] - the largest shear modulus value obtained when applying shear strain levels smaller than 10^{-4} percent.

Hysteresis loop - a plot of shear stress (load) as a function of shear strain (deformation) after applying one complete cycle during the torsional shear (TS) test. The area of the loop is the dissipated energy within the specimen.

Modulus reduction curve - a plot of modulus ratio, G/G_{max}, as a function of shear strain. Modulus reduction curve is used to model the characterization of the soil specimen.

3.4. Summary of Test Method

A soil specimen in the Stokoe-type RCTS apparatus is exposed to fixed-free boundary conditions (with a fixed base and a free top). Torsional excitation, at various frequency and amplitude levels, is applied to the top of the specimen by a coil-magnet drive mechanism while the bottom of the specimen is held fixed to a rigid base pedestal.

3.4.1. RC Test

The basic operational principle of the RC test is to vibrate a cylindrical soil specimen in first-mode torsional motion. The top and bottom of the specimen are rigidly fixed to the base pedestal and top cap that each have roughened contact surfaces to enhance fixidity. A drive plate is firmly attached to the top cap with four screws, and the entire top system is free to move during the cyclic torque application. Harmonic torsional excitation with a constant maximum torque amplitude is applied to the top of the specimen over a range of frequencies, and the variation of the acceleration amplitude at the top of the specimen is obtained. Determinations of the resonant frequency and maximum amplitude of vibration are then collected from the response curve. These values are combined with 1) equipment characteristics and 2) the specimen parameters (height, diameter, mass) to calculate the shear wave velocity (V_s), the shear modulus (G), and the shear strain amplitude (γ). Material damping (D) is evaluated from the dynamic response using

either the free-vibration decay curve or the half-power bandwidth method. The free-vibration delay curve is recorded by shutting off the driving force after the specimen has undergone steady state motion at the resonant frequency.

3.4.2. TS Test

Slow cyclic torsional loading with a given frequency and amplitude, generally below 10 Hz and 10V, is applied at the top of the specimen during the torsional shear test. A stress-strain hysteresis loop is determined by measuring the torque-twist response of the specimen. Proximeters are used to measure the angle of twist while the amount of torque is inferred from the amount of voltage applied to the coil. The secant shear modulus is calculated from the slope of a line through the two end-points of the hysteresis loop. The material damping ratio is determined from the hysteresis loop as the ratio of the energy dissipated in one cycle of loading to the peak strain energy stored during the cycle times a factor of $1/4\pi$.

3.5. Significant and Use

3.5.1. The shear modulus and damping ratio can be determined from the RCTS test for 1) specimens with different void ratio values, and for 2) specimens subjected to different effective stress states, excitation frequencies, strain amplitudes, number of loading cycles, etc. These parameters are useful for calculations involving dynamic response and soil-structure interaction.

3.5.2. The calibration for this test is complicated. Several calibrations are involved, and an improper calibration value may lead to misleading results. Therefore, it is recommended that at least two different calibration methods are utilized to assure accurate results from the calibration. The biggest limitation of the test is the problem related to non-uniform levels of stress and strain across the radius of soil specimen. An equivalent radius of 0.82 is commonly used for shearing

strain values less than 10^{-3} percent and 0.79 for shearing strain values equal to 0.1 percent. These typical equivalent values are selected to account for non-uniform stress-strain conditions (Chen and Stokoe 1979).

3.6. Apparatus

3.6.1. General - A schematic of the RCTS testing apparatus is shown in Figure 3.1.

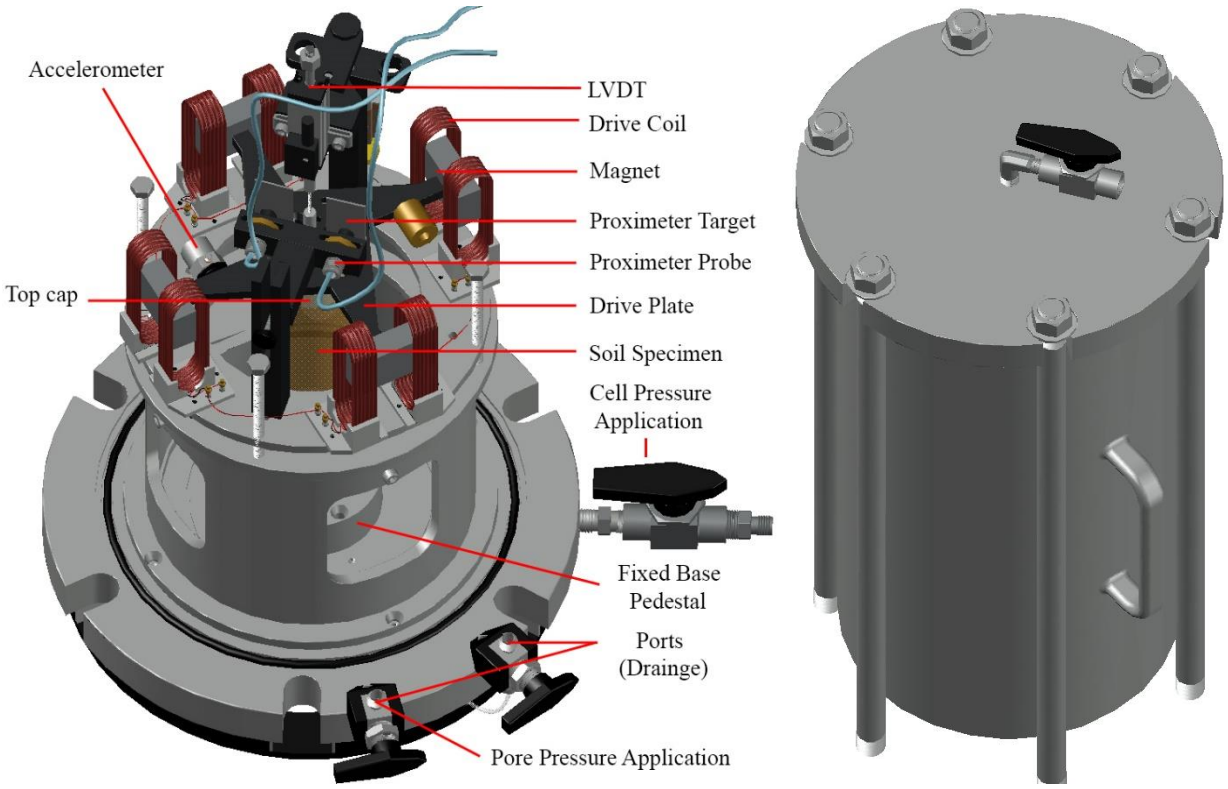

Figure 3.1. Resonant column torsional shear device, a) interior of device overview, and b) confinement chamber.

3.6.2. Driving System - The driving system consist of four magnets, eight drive coils and a drive plate. The alignment of the magnets should be adjusted so that the magnets are centered in the middle of the drive coil, without touching the coil, to avoid compliance problems.

3.6.3. *Accelerometer* - Torsional vibrations of the drive plate within the frequency range from 20 Hz to 200 Hz are sensed using an accelerometer. The accelerometer is only utilized during the RC testing. The accelerometer shall be calibrated before use and shall be countered balanced on the drive plate.

3.6.4. *Proximeter* - The frequency of motion used in the TS test is typically within the 0.01 Hz to 10 Hz range which is too low to be detected by the accelerometer that is used for the RC test. Therefore, a set of proximeters is used. To obtain appropriate TS results at small-strain test, the air gap distance between the proximeter probes and the proximeter target should not be larger than 0.5cm.

3.6.5. *Specimen Axial Deformation Measurement* – A linear variable differential transducer (LVDT) or direct current displacement transducer (DCDT) is used to measure the axial deformation of the specimen due to consolidation during confinement or due to excess pore water pressure development during shearing. The LVDT or DCDT mounts to the coil jacket and touches the drive plate at center of the drive plate. The LVDT or DCDT should be calibrated prior to performing the test.

3.6.6. *Pressure Measurement Devices* - Pressure transducers are attached to the pressure ports to measure the chamber confining pressure (cell pressure) and the pore water pressure. The pressure transducers should be calibrated prior to performing the test.

3.6.7. *Low Pass Signal Filtering* – A low pass filter is used to remove the noise in the signals, especially when the signal amplitude of the output is low.

3.6.8. *Confinement System* - The confining chamber is made of stainless steel to avoid the possibility of magnetic reactions between the magnets and the confining system. This chamber is also capable of withstanding high-pressure levels.

3.6.9. *Fluid Bath* – Silicon oil is placed into the acrylic cylinder that surrounds the base pedestal to form a silicon fluid bath. The silicon fluid bath is utilized to prevent air diffusion from the confining chamber through the membrane to the soil specimen during the RCTS test.

3.6.10. *Filter Paper* - Filter paper is used to cover the holes in the top part of the base pedestal. The filter paper helps to avoid clogging in the port during the pore pressure application. The filter paper shall be of a type that does not dissolve in water.

3.6.11. *Membrane* - The soil specimen is encased in a membrane. The membrane should be inspected prior to use to make sure there are no holes or flaws. The membrane should be extended from the specimen top cap to the specimen base pedestal. The inside of the membrane should be sealed, by application of O-rings around the top cap and base pedestal. For high angularity sand, the use of two membranes should be considered.

3.6.12. *Specimen Top Cap and Base Pedestal* - The bottom part of the top cap and the top part of the base pedestal are roughened to create fixity between the soil specimen and the pedestal when applying torque.

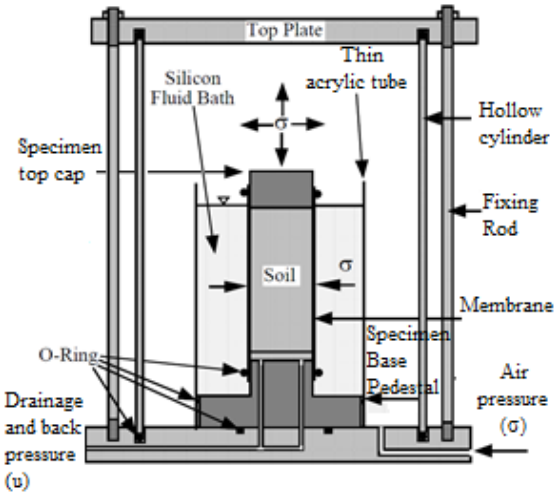

Figure 3.2. Simplified cross-section configuration of the confinement system and testing (modified from Hwang, 1997).

3.7. Test Specimen Preparation

3.7.1. General – ASTM Test Method D3999 (2011) may be used for specimen preparation.

3.7.2. Specimen Size - Specimens shall be cylindrical and have a minimum diameter of 33mm (1.3 in.). The average height-to-diameter ratio shall be between 2.0 and 2.5. The largest particle size shall be smaller than 1/6 the specimen diameter. If, after the completion of a test, it is found based on visual observation that oversized particles were present, an appropriate statement shall be made in the report of the test data under the remarks section.

3.7.3. Intact Specimens - Prepare intact specimens from large intact samples or from samples secured in accordance with ASTM D1587 (2015) or other acceptable intact tube sampling procedures. Samples shall be preserved and transported in accordance with the practices for Group C samples in ASTM D4220 (2014). Specimens obtained by tube sampling may be tested without trimming except for cutting the end surfaces plane and perpendicular to the longitudinal axis of the specimen, provided soil characteristics are such that no significant disturbance resulted from sampling. Handle specimens carefully to minimize 1) disturbance, 2) changes in cross section, or 3) change in water content. If compression or any type of noticeable disturbance would be caused by the extrusion device, split the sample tube lengthwise or cut the tube into suitable sections to facilitate removal of the specimen with minimum disturbance.

Prepare trimmed specimens, in an environment such as a controlled high-humidity room, where soil water content change is minimized. Where removal of pebbles or crumbling resulting from the trimming process causes voids on the surface of the specimen, carefully fill the voids with remolded soil obtained from the trimmings. Up to

ten percent of the surface area can be refilled. If the sample can be trimmed with minimal disturbance, a vertical trimming lathe may be used to reduce the specimen to the required diameter. After obtaining the required diameter, place the specimen in a miter box, and cut the specimen to the final height with a wire saw or other suitable device. Perform one or more water content determinations on material trimmed from the specimen in accordance with ASTM D2216 (2010).

3.7.4. *Reconstituted (Compacted) Specimens* - Soil required for reconstituted specimens shall be thoroughly mixed with sufficient water to produce a desired water content. If water is added to the soil, store the material in a covered container for at least 16h prior to compaction. Reconstituted specimens may be prepared by compacting material in at least three layers using a split mold of circular cross section having dimensions meeting the requirements enumerated in 3.7.2. Specimens may be reconstituted to the desired density by either *1*) kneading or tamping each layer until the accumulative mass of the soil placed in the mold is reconstituted to a known volume; or *2*) by adjusting the number of layers, the number of tamps per layer, or the force per tamp to achieve a desired level of energy input. The top of each layer shall be scarified prior to the addition of material for the next layer. The tamper used to compact the material shall have a diameter equal to or less than one half the diameter of the mold. After a specimen is formed, with the ends perpendicular to the longitudinal axis, remove the mold and determine the mass and dimensions of the specimen. Perform one or more water content determinations on excess material used to prepare the specimen in accordance with ASTM D2216 (2010).

3.7.5. *Reconstituted (Slurry Consolidated) Specimens* – Soil required for slurry consolidated specimens shall be thoroughly mixed with sufficient water to produce a desired water

content slurry. The slurry was then poured into a slurry consolidometer and subjected to a vertical effective stress of 137.8 kPa. The stress of 137.8 kPa is withheld until the specimens reach 100-percent average degree of consolidation. By recording the vertical displacement as a function of time and using the log time method or Taylor square root method, the permeability of the specimen can be determined. Then the specimens were extruded from the slurry consolidometer to perform the test.

3.7.6. Reconstituted (Sand) Specimens Using Air Pluviation Method – A small vacuum is applied to the split mold to keep the sample together during reconstitution. The sand is poured to the split mold using the funnel, and it should be compacted to at least three layers. The difference in weight of bowl before and after pouring is equal to the sample weight. When the target height is obtained, the membrane is pulled over the top cap and sealed with an O-ring. The diameter and height of sand specimen are then recorded.

3.8. Calibration and Standardization

3.8.1. Drive Plate Mass Polar Moment of Inertia (J_o): The top portion of the soil specimen is not free to move independently because the specimen top cap and drive plate system, attached to the top of the soil specimen, creates additional mass on top of the specimen. Therefore, it is necessary to calibrate the mass polar moment of inertia of the specimen top cap and the drive plate assembly to account for this issue in an RC test. The mass polar moment of inertia for the specimen top cap, J_t, is calculated by using Equation 3.1:

$$J_t = \frac{m_t d_t^{\,2}}{8} \qquad \text{(Equation 3.1)}$$

where:

J_t = mass polar moment of inertia for the specimen top cap [kg·m^2]

m_t = mass of the specimen top cap [kg], and

d_t = diameter of the specimen top cap [m].

Because the shape of the drive plate is more complex than the specimen top cap, aluminum calibration specimens and stainless-steel masses with known geometric and material properties are utilized to experimentally determine the mass polar moment of inertia of the drive plate, J_o. The value of J_o and K_{metal} are determined from Equation 3.2 and Equation 3.3, respectively:

$$K_{metal} = \frac{4\pi^2 \Delta J_i (f_r f_{r,i})^2}{(1-D^2)(f_r^2 - f_{r,i}^2)} \quad \text{(Equation 3.2)}$$

$$f_{r,i} = \frac{1}{2\pi}\sqrt{\frac{K_{metal}}{J_o + J_t + \Delta J_i}}\sqrt{1-D_i^2} \quad \text{(Equation 3.3)}$$

where:

J_o = drive plate mass polar moment of inertia [kg·m^2],

K_{metal} = torsional stiffness of the metal calibration specimen [N·m/rad],

f_r = resonant frequency when performing RC test with the metal calibration specimen without added mass [Hz],

$f_{r,i}$ = resonant frequency when performing RC tests with the metal calibration specimen and with added mass number i [Hz],

ΔJ_i = polar moment of inertia of the added mass number i [kg·m^2], and

D = material damping ratio of the specimen rod (D ≈ 0 percent).

3.8.2. Proximeter Calibration Factor, K_p (rad/V):

3.8.2.1. Proximeter Linear Calibration Method

To determine the proximeter calibration factor, the output voltages of the proximeters are measured at 0.127 mm intervals or 0.254 mm intervals as the proximity probe tips move linearly

toward or away from the proximeter target. The slope of the trendline in the change in output voltage and the gap between proximeter targets plot (Figure 3.3) will be the linear proximeter calibration factor, $K_{p,linear}$.

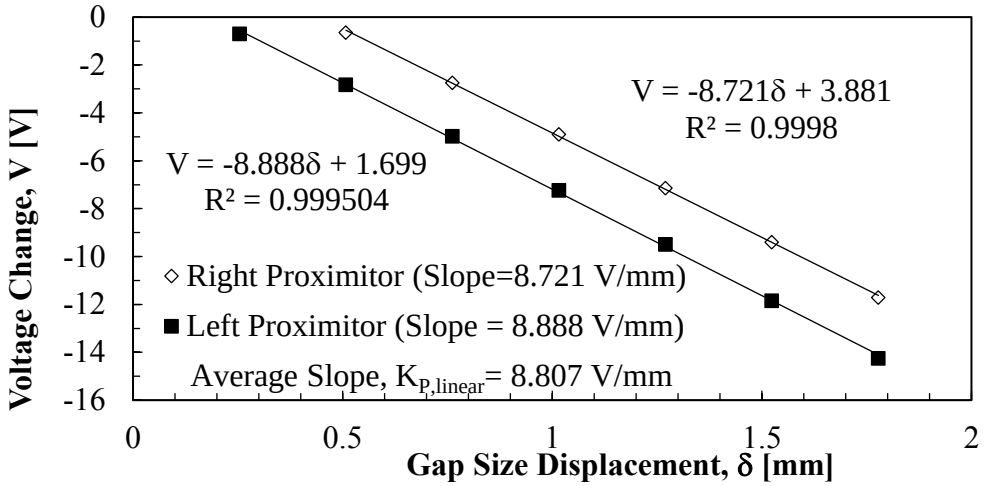

Figure 3.3. Plot of proximeter voltage change as a function of gap size displacement for the left and right proximeter.

The linear proximeter calibration factor is obtained from the averaged results from the left and right proximeter probes. The obtained linear calibration factor is inverted and divided by two to account for the use of two probes together. To convert the displacement unit to rotation unit, the obtained calibration factor is divided to the radius from the center of rotation to the center of the tip of each proximity probe, r_P. The arctangent value of obtained rotation unit is the final proximeter calibration factor, K_P. The proximeter calibration factor, K_P, is determined from Equation 3.4.

$$K_P = \tan^{-1}\left(\frac{r_P}{2 \cdot K_{P,linear} \cdot}\right) \qquad \text{(Equation 3.4)}$$

where:

K_P = Proximeter calibration factor [rad/V],

r_P = radius from the center of rotation to the center of the tip of each proximity probe [mm], and

$K_{P,linear}$ = linear proximeter calibration factor obtained from the proximeter voltage change as a function of gap size displacement [V/mm].

Detailed calculations of the determination of the calibration factor are shown in Section 4.2.1 and Section 2 in Appendix.

3.8.2.2. Proximeter Rotational Calibration

Another way to determine the proximeter calibration factor is through a rotational calibration. The rotational calibration is performed by rotating the proximeter probes with a controlled rotation. The output voltages of the proximeters are measured at every 0.25 or 0.5 degree intervals as the proximeter probes rotate toward or away from the respective proximeter target. The slope of the linear trendline in the change in voltage and the proximeter rotation angle plot is the calibration factor (Figure 3.4).

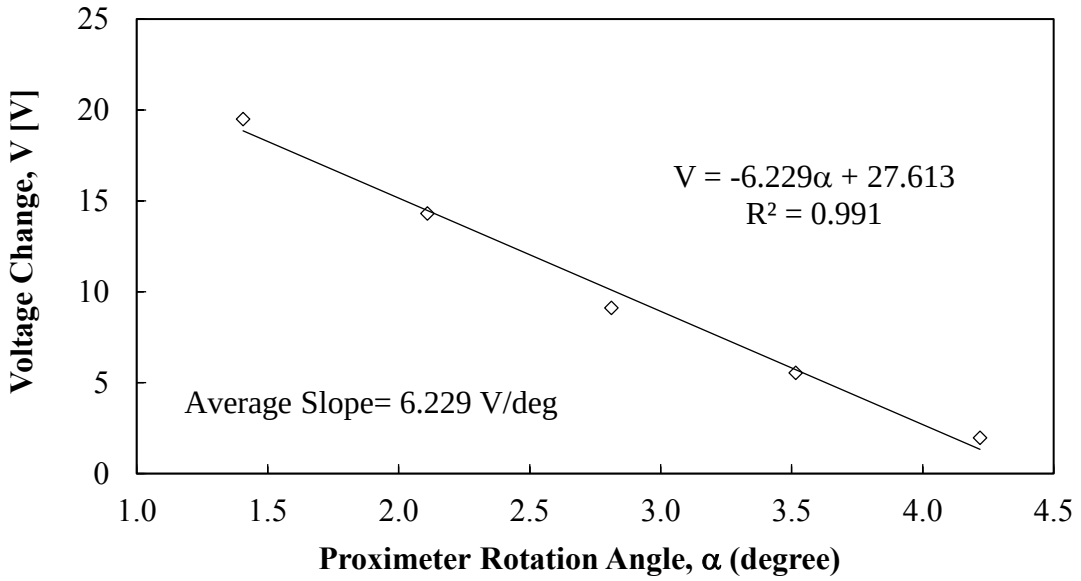

Figure 3.4. Plot of proximeter voltage change as a function of proximeter rotation angle.

3.8.3. Torque Calibration Factor, K_T [N·m/V]

3.8.3.1. Calibration using the Calibration Specimen

The calibration specimens with known geometries and properties are placed in the devices in place of the soil specimen. After setting up the drive system, the TS tests were performed at frequency values of 0.1Hz, 0.5Hz, 1Hz and 2Hz respectively. At each frequency, the drive coil was driven with the following amounts of supplied voltage, V_T: 30mV, 75mV, 150mV, 300mV, 600mV, 1200mV, 2400mV, and 3000mV. For each supplied voltage, the maximum proximeter values, V_P, are recorded. Because the torsional stiffness of the calibration specimens and the proximeter calibration factor are known, the torque calibration factor can be determined by using Equation 3.5.

$$K_T = \frac{V_p K_p K_{metal}}{V_T} \qquad \text{(Equation 3.5)}$$

where:

K_T = Torque calibration factor [N·m/V],

K_p = Proximeter calibration factor [rad/V],

K_{metal} = Torsional stiffness of the metal calibration specimen [N·m/rad],

V_p = Proximeter output voltage [Volt], and

V_T = Coil excitation (torque) output voltage [Volt].

3.8.3.2. Calibration using Torque Sensor

The second way to determine the torque calibration is to use a torque sensor to directly measure the torque of the drive system. The torque sensor was mounted to the top of the drive plate. The torque sensor has capability to measure the torque of the drive plate. The torque calibration

factor was obtained from the ratio of measured torque and the measured applied voltage. The torque sensor shall be calibrated properly prior to performance of the aforementioned calibration.

3.9. Procedure

3.9.1. Inspection:

3.9.1.1. Inspect if there are any flaws, holes or leaks in the membrane. If yes, a new membrane must be used.

3.9.1.2. Inspect the drainage line to make sure there is no clogging. If yes, clean the drainage line using high pressure and water.

3.9.1.3. Filter paper is used to cover the holes in the top part of the base pedestal.

3.9.2. *Specimen Preparation* - Trim the sample to the desired height and diameter, then place the soil specimen on the base pedestal. Place the specimen top cap on top of the specimen. Use a membrane expander to place the membrane around the specimen. The specimen is then sealed by placing O-rings around the membrane at the base pedestal and top cap. A thin coat of silicon grease may be used around the diameter of the specimen top cap and base pedestal to aid in sealing the membrane to the base pedestal and specimen top cap.

3.9.3. *Apply vacuum pressure for specimens that are not self-supporting* – A small vacuum pressure maybe applied (<14 kPa or <2 psi) to the pore pressure lines to prevent the specimen from collapsing.

3.9.4. *Silicon Fluid Bath* - A cylindrical tube, which fits around the base pedestal and seals against the base pedestal, is placed around the soil specimen and filled with silicon oil to prevent any air pressure migration through the membrane and into the specimen.

3.9.5. *Attachment of the Drive System* – The drive plate system must be properly adjusted to obtain accurate results. First, the plane of the driving system should be placed horizontally to generate uniform torsional force at the top of the specimen. Second, the magnets should be centered in the drive coils to avoid compliance issues. Finally, the air gap distance between the proximeter probes and the proximeter target should not be further than 0.5cm to obtain proper TS results.

3.9.6. *Placement of Confining Chamber* - Apply a thin coat of silicon grease to the O-rings located in the confinement chamber base and confinement chamber lid to ensure a proper seal and prevent leaks from the confinement chamber.

3.9.7. *Application of Proper Pressures*

3.9.7.1. *Confining Pressure* - Use the cell pressure regulator to apply air pressure into the chamber, the confining pressure is measured and recorded by using the cell pressure transducer.

3.9.7.2. *Pore Water Pressure* - Use the pore pressure pump to apply and maintain the pore water pressure inside the membrane and within the soil specimen. The pore pressure is measured and recorded by utilizing the pore water pressure transducer mounted onto the pore water pressure valve on the base of the chamber.

3.9.7.3. *Application Back Pressure to Saturate the Soil Specimen* - The detailed process of applying back pressure can be consulted in ASTM 4767 (2011).

3.9.7.4. *Adjustment of the Effective Stress* - The confining pressure and pore water pressure should be adjusted together to obtain the targeted effective stress. The effective stress is equal to the difference between the measured confining pressure and the measured pore water pressure. The pore water pressure must never exceed the confining pressure.

3.9.8. *Performing the RC and TS Tests:*

3.9.8.1. *Effective Stress* – The test pressure is selected for each test; the mean effective confining pressure [$\sigma'_o = (\sigma'_v + 2\sigma'_h)/3$] is selected as the required effective stress state. The first sub-test should be performed with a small effective stress of approximately $0.25\sigma'_o$ on the sample to keep sample disturbance at a minimum. The next sub-tests are typically conducted at effective stress levels of $0.5\sigma'_o$, $1.0\sigma'_o$, $2.0\sigma'_o$ and $4.0\sigma'_o$.

3.9.8.2. *Testing Schedule for Test* – Perform one small-strain RC test and one small-strain TS test by applying low excitation voltage (approximately 0.3 mV for RC test and 30mV for TS test) to obtain the maximum shear modulus. The small-strain test shall have the shear strain less than 10^{-4} percent to obtain the maximum shear modulus. Because the results from RC tests are reliable at the shear strain levels from 10^{-6} percent to 10^{-2} percent, depending upon the stiffness of the sample, the entire RC tests are performed after the small-strain tests. The RC tests should be performed up to a strain level of 10^{-2} percent. Each small-strain RC test check, a RC test with the same excitation voltage used to perform small-strain RC test, should be conducted after driving the coils with higher amounts of excitation voltage (greater than the excitation voltage in the small-strain RC test). The purpose of performing a small-strain RC test check is to account for the reduction in the maximum shear modulus. After the RC tests, wait for a certain amount of time (depend on soil type, typically two hours for sand and one day for clay) for the soil specimen to recover then perform the TS tests. Because the TS results are reliable after the shear strain levels from 10^{-2} percent to 1 percent, the TS tests are performed in this range. Each small-strain RC test should also be performed after each TS test to account for the change of the maximum shear modulus after driving the coils with higher amounts of excitation voltage.

3.10. Calculation or Interpretation of Results

3.10.1. General- Calculations for the RC and TS tests require the apparatus calibration factors, the specimen mass, and dimensions of the soil specimen.

3.10.2. Soil Mass Density- The soil mass density, ρ, is obtained using Equation 3.6:

$$\rho = \frac{4M}{\pi D^2 L} \qquad \text{(Equation 3.6)}$$

where:

M = total mass of soil specimen [kg],

D = diameter of soil specimen [m], and

L = Length of soil specimen [m].

3.10.3. RC test calculation:

3.10.3.1. Mass polar moment of inertia of the soil specimen. The mass polar moment of inertia of the soil specimen, J, is obtained using Equation 3.7:

$$J = \frac{MD^2}{8} \qquad \text{(Equation 3.7)}$$

3.10.3.2. Shear wave velocity of the soil specimen. The shear wave velocity of the soil specimen, V_s, should be calculated by using the one-dimensional wave propagation equation shown as Equation 3.8. The shear wave velocity can be calculated by utilizing a solver function to set Equation 3.8 equal to zero.

$$\frac{J}{J_o + J_t} - \frac{\omega L}{V_s}\tan\left(\frac{\omega L}{V_s}\right) = 0 \qquad \text{(Equation 3.8)}$$

where:

J = mass polar moment of inertia of the soil specimen [kg·m^2],

J_o = mass polar moment of inertia for the drive plate [kg·m^2],

J_t = mass polar moment of inertia for the specimen top cap [kg·m^2],

ω = resonant frequency of the soil specimen [rad/s], and

L = length of the soil specimen [m] at the time of rotation.

3.10.3.3. Shear modulus of the soil specimen. The shear modulus of the soil specimen, G, should be calculated using Equation 3.9 after finding ρ and V_s from Equations 3.6 and 3.8, respectively.

$$G = \rho V_s^2 \qquad \text{(Equation 3.9)}$$

3.10.3.4. Damping ratio of the soil specimen. The damping ratio of the soil specimen, δ, is found utilizing the half-power bandwidth method or the free vibration curve.

3.10.3.4.1. The half-power bandwidth method. The damping ratio, δ, should be calculated using Equation 3.10 and is graphically displayed in Figure 3.5.

$$\delta = \frac{f_2 - f_1}{2 f_r} \qquad \text{(Equation 3.10)}$$

where:

f_1, f_2 = the frequencies recorded at the value of 0.707 times the maximum amplitude of vibration [Hz].

f_r = resonant frequency

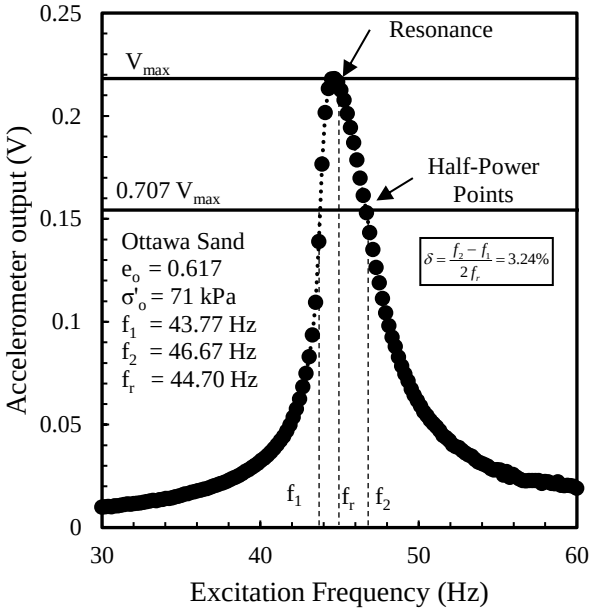

Figure 3.5. Half power bandwidth method using to calculate the damping ratio.

3.10.4.2. The free-vibration decay method. The damping ratio, δ, should be calculated using Equation 3.11. The free-vibration decay curve was recorded by shutting off the driving force after the specimen was undergoing steady-state motion at the resonant frequency. The free vibration decay method (Figure 3.6) is recommended for use when performing high amplitude RC test where the response curve is no longer symmetrical.

$$\delta = \frac{1}{n} \ln \left(\frac{A_1}{A_{n+1}} \right) \qquad \text{(Equation 3.11)}$$

where:

A_1 = amplitude of vibration for first cycle after shutting off the driving force while at resonance,

A_{n+1} = amplitude of vibration for $(n+1)^{th}$ cycle of free vibration, and

n = number of free vibration cycles which must be 10 or less.

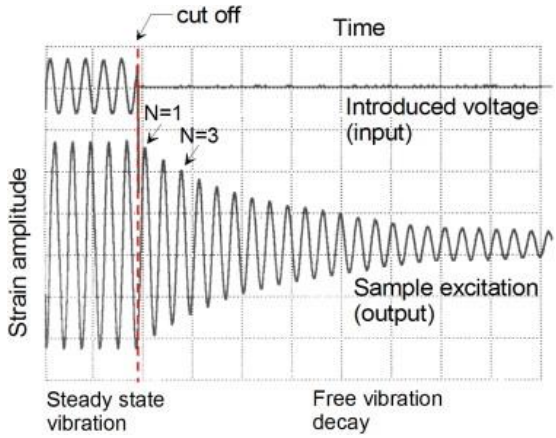

Figure 3.6. Free vibration decay method using to calculate the damping ratio (Senetakis, 2015).

3.10.3.1. Shearing strain calculation. The shearing strain, γ, should be calculated using Equation 3.12:

$$\gamma = \frac{g}{r_a}(CAF)(CF)\frac{(a)(D/2)(ER)}{(L)(f_r^{\,2})}100\% \qquad \text{(Equation 3.12)}$$

where:

g = acceleration of gravity (=9.81 m/s^2),

r_a = the distance from the location of accelerometer to the center of specimen (m),

CAF = charge Amplifier Factor (if not available, can use CAF= 0.4 [g/V],

CF = conversion factor from RMS Voltage to Single Amplitude Voltage $\left(=\frac{\sqrt{2}}{(2\pi)^2}\right)$,

a = accelerometer output [V],

f_r = resonant frequency [Hz], and

ER = equivalent radius (=0.82 for shearing strain less than 10^{-3} percent and =0.79 for shearing strain equals to 0.1 percent).

3.10.4. TS test calculation

3.10.4.1.1. Equivalent shear strain. The equivalent shear strain, γ_{eq}, should be calculated using Equation 3.13:

$$\gamma_{eq} = \frac{ER}{2}(V_p)(K_p)\left(\frac{D}{L}\right) \quad \text{(Equation 3.13)}$$

where:

V_p = proximeter output voltage [V], and

K_p = proximeter calibration factor [rad/V].

3.10.4.1.2. Area moment of inertia. The area moment of inertia, J_p, should be calculated using Equation 3.14:

$$J_p = \frac{\pi D^4}{32} \quad \text{(Equation 3.14)}$$

3.10.4.1.3. Equivalent shear stress. The equivalent shear stress, τ_{eq}, should be calculated using Equation 3.15:

$$\tau_{eq} = \frac{ER}{2}(V_T)(K_T)\left(\frac{D}{J_p}\right) \quad \text{(Equation 3.15)}$$

where:

V_T = coil excitation (torque) output voltage [V], and

K_T = torque calibration factor [N·m/V].

3.10.4.4. Shear modulus. The shear modulus, G, should be calculated using Equation 3.16:

$$G = \frac{\tau_{eq}}{\gamma_{eq}} \quad \text{(Equation 3.16)}$$

Typically, the secant modulus, G_{sec}, is found from the hysteresis loop

3.10.4.5. Hysteretic damping ratio. The hysteretic damping ratio, λ, is calculated utilizing Equation 3.17 and is displayed in Figure 3.7:

$$\lambda = \frac{A_{loop}}{4\pi(A_{triangle})} \qquad \text{(Equation 3.17)}$$

where:

A_{loop} = area of the hysteresis loop

$A_{triangle}$ = area of the the cross triangle

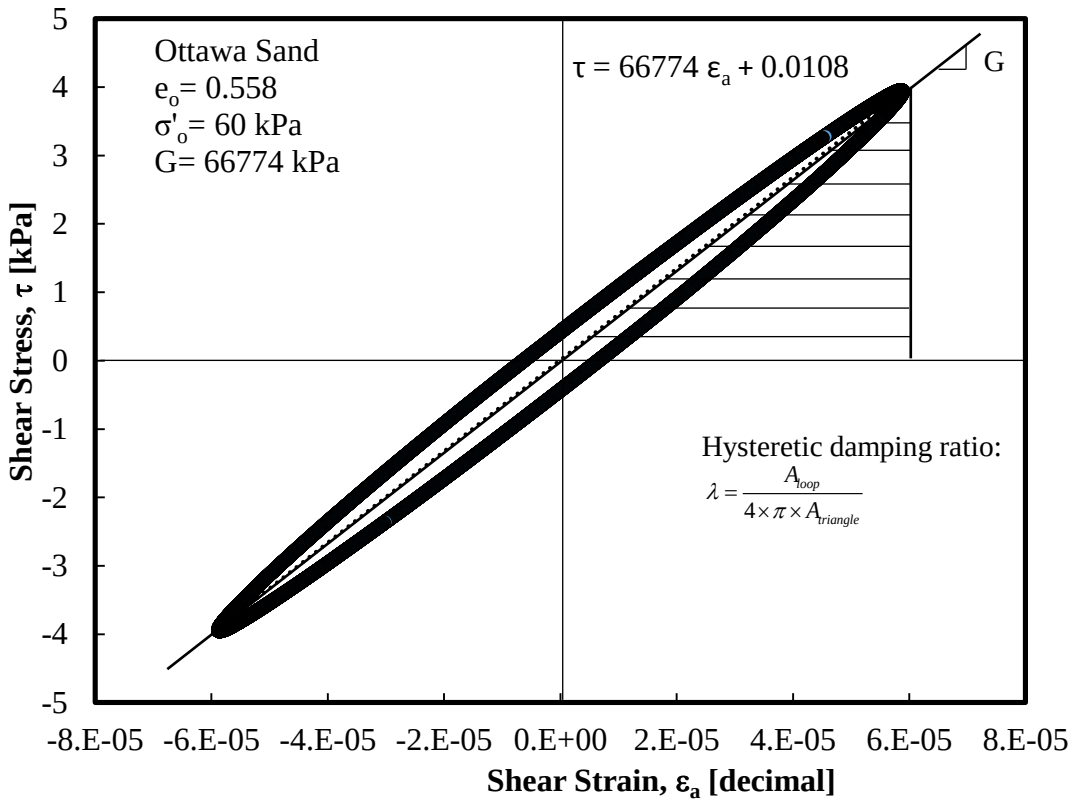

Figure 3.7. Typical hysteresis loop generated during torsional shear test.

3.10.4.6. Normalized modulus reduction curve. The normalized shear modulus, G/G_{max}, is determined by dividing the obtained shear modulus at the RC or TS tests with the shear modulus

value from the following up small-strain RC test check. The plot of the normalized shear modulus as a function of shear strain is the normalized reduction curve as displayed in Figure 3.8.

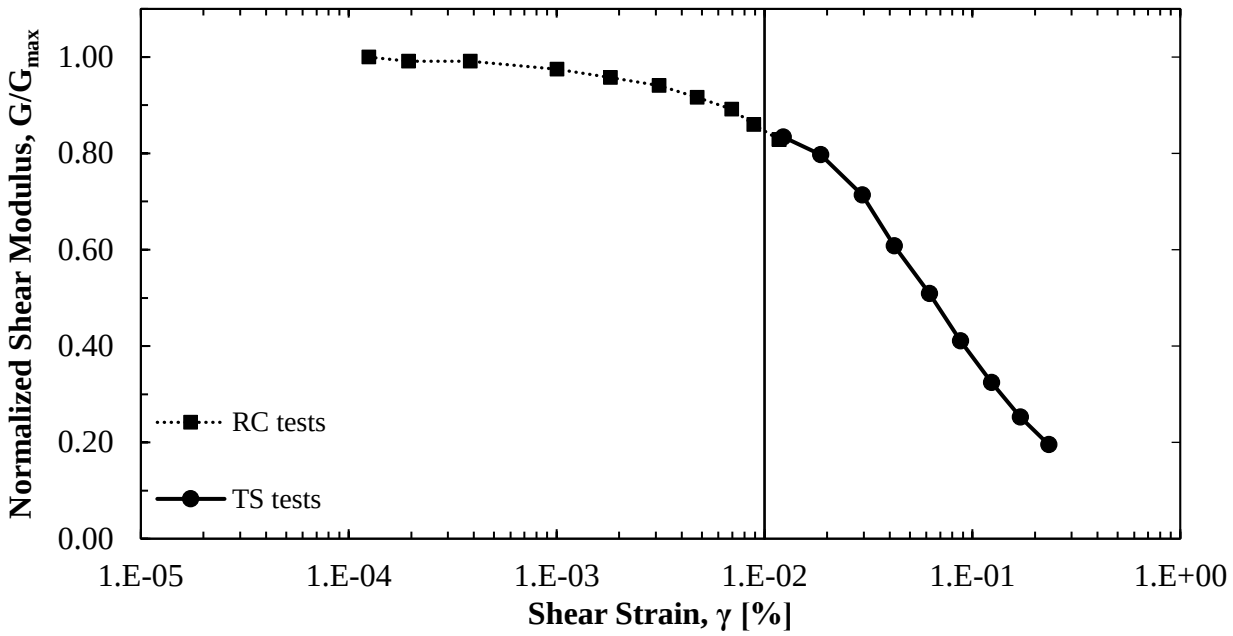

Figure 3.8. Typical normalized modulus reduction curve.

3.11. Report

Report the following information:

3.11.1. Date and time of test, performance operator name, project name, boring log number, specimen number.

3.11.2. Apparatus name, model number, and serial number.

3.11.3. Calibration information: Mass polar moment of inertial for the top platen (J_t), polar moment of inertia of the added mass number i (ΔJ_i), resonant frequency in Hz with added mass number i ($f_{r,i}$), mass polar moment of inertia of the drive plate (J_o), the proximeter calibration factor (K_p), the torque calibration factor (K_T).

3.11.4. Initial and final length, diameter, weight, void ratio and moisture content of the specimen. A visual description and origin of the soil shall be given, including name, group symbol, and whether intact or remolded.

3.11.5. The stress state shall be given including the total stresses, pore water pressure, drainage conditions, and the procedures used to measure applied stresses, pore pressures, length change and volume change.

3.11.6. For the TS test, record the cycle number (typically perform for 10 cycles), frequency (typically perform with 0.5Hz) and drive coil or proximeter amplitude for each test.

3.11.7. For the RC test, record the drive coil voltages used to perform the test, the frequency, accelerometer output and the phase angle.

3.11.8. Equivalent radius used to calculate the average shear strain if different from recommendation (0.82 for shearing strain less than 10^{-3} percent and 0.79 for shearing strain equals to 0.1 percent).

3.11.9. Resonant frequency, shear strain, shear modulus and damping ratio.

3.11.10. Plot of the modulus reduction curve and damping curve (normalized shear modulus and damping ratio as a function of shear strain).

3.12. Precision and Bias

3.12.1. Test data on precision is not presented due to the nature of the materials tested by this test method. It is either not feasible or too costly at this time to have ten or more laboratories participate in a round robin testing program. Also, it is either not feasible or too costly to produce multiple specimens that have uniform physical properties. Any variation observed in the data is just as likely to be due to specimen variation as to operator or laboratory testing variation.

3.12.2. Subcommittee D18.09 is seeking any data from the users of this test method that might be used to make a limited statement on precision.

3.12.3. *Bias* - There is no accepted reference value for this test method, therefore, bias cannot be determined. The variability of soil and resultant inability to determine a true reference value prevent the development of a meaningful statement of bias. The subcommittee is seeking pertinent data from users of this test method to establish the precision and bias of this test method.

3.13. Keywords

3.13.1. Amplitude; confining pressure; damping; dynamic loading; frequency; free vibration curve; half-power bandwidth; laboratory tests; non-destructive tests; resonance; shear modulus; shear modulus reduction curve; soils; small shear strain; shear strain; shear stress; torsional shear test;

CHAPTER 4: METHODS USED FOR AND RESULTS OBTAINED FROM THE CALIBRATION PROCEDURE

4.1. Chapter Overview

The results obtained from the calibration of the RCTS devices at the University of Arkansas (UofA) are presented in this chapter. The calibration included determination of: the drive plate mass polar moment of inertia (Section 4.1), the proximeter calibration factor (Section 4.2), and the torque calibration factor (Section 4.3). The method used to determine the drive plate mass polar moment of inertia, J_o followed the work performed by Deschenes (2015). The methods used to determine the proximeter calibration factor, K_P, and torque calibration factor, K_T, followed the work performed by Scheer (1992) and Hwang (1997).

4.2. Drive Plate Mass Polar Moment of Inertia, J_o

Three calibration specimens, composed of 6061-T6 Aluminum, were tested with different added mass conditions (no mass, one mass, two masses, and three masses) to calibrate the RCTS devices at the UofA. Specifically, the specimens were used for the J_o calibration and for the K_T calibration. Each of the individual added masses was comprised of a 303 Stainless Steel puck of approximately equal dimensions, mass, and polar moment of inertia. Each of the individual three candle stick calibration specimens were of equal height, base, and top platen thicknesses. The diameter of the shaft of each of the individual candlestick specimens differed.

The three candlestick calibration specimens, along with the three additional pucks, were purchased by the UofA from Trautwein Soil Testing Equipment, Co, for the purpose of calibrating the RCTS devices at the UofA. Identical specimens were also purchased by the Norwegian Geotechnical Institute (NGI) to calibrate the device at NGI. Trautwein provided specifications for the specimen and plates, which were also measured by the author; the

measured results were in agreement with those provided by Trautwein. A schematic of a typical calibration specimen (UA Calibration Specimen 3) is illustrated in Figure 4.1. The physical dimensions and material properties of three candlestick calibration specimens and three additional pucks are presented in Table 4.1. By performing RC tests on the three calibration rods with three different added mass conditions (no mass, one added mass, two added masses and three added masses), the resonant frequency and damping ratio were obtained for each condition (Table 4.2). The J_o and K_{metal} values that were obtained by simultaneously solving the Equation 3.2 and Equation 3.3, respectively, are presented in Table 4.3. An example calculation of J_o and K_{metal}, using the data collected at the UofA, is provided in Appendix A- Section 1.

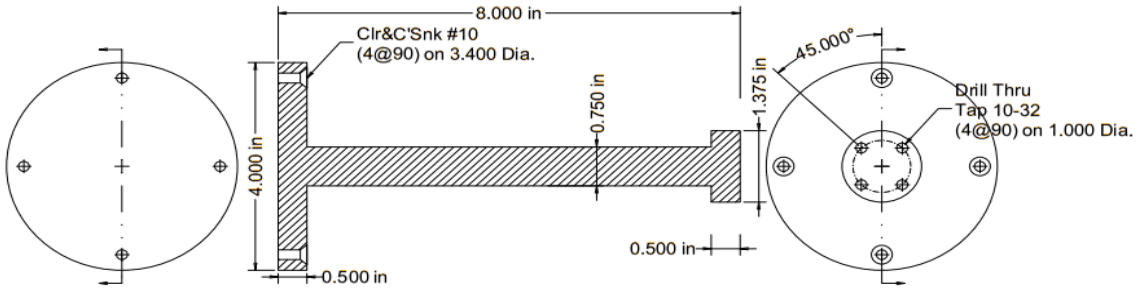

Figure 4.1. Schematic of RCTS calibration specimen (from Trautwein, 2008).

Table 4.1. Physical dimensions and material properties of calibration specimens at the UofA (from Deschenes, 2015).

Calibration Specimen	Material	Density	Diameter		Polar Mass Moment of Inertia	
		ρ	Rod, d_r	Top Plate, d_t	Rod, J_r	Top Plate, J_t
		$g \cdot cm^{-3}$	mm	mm	$kg \cdot m^2$	$kg \cdot m^2$
1	6061-T6 Al	2.700	9.53	34.93[a]	3.900×10^{-7}	5.011×10^{-6}
2	6061-T6 Al	2.700	15.88	34.93[a]	3.009×10^{-6}	5.011×10^{-6}
3	6061-T6 Al	2.700	19.05	34.93[a]	6.240×10^{-6}	5.011×10^{-6}
M1	Stainless Steel	7.806	-	71.12[b]	-	1.853×10^{-4}
M2	Stainless Steel	7.806	-	71.12[b]	-	1.853×10^{-4}
M3	Stainless Steel	7.806	-	71.12[b]	-	1.853×10^{-4}

[a]Height of Top Plate of Calibration Specimen (h=12.7mm= 0.5in.)

[b]Height of Added Mass (hm=9.525mm); masses applied sequentially/simultaneously

Table 4.2. Results of calibration testing at UofA (from Deschenes, 2015).

Added Mass	31-Hz Specimen		85-Hz Specimen		120-Hz Specimen	
	F_m (Hz)	D (%)	F_m (Hz)	D (%)	F_m (Hz)	D (%)
NM[a]	32.690	0.466%	88.148	0.231%	125.412	0.150%
M1[b]	31.692	0.484%	86.452	0.204%	120.280	0.248%
M2	30.792	0.470%	83.975	0.178%	118.414	0.168%
M3	29.884	0.443%	81.125	0.255%	113.057	0.338%

[a]NM Represents Specimen with No Additional Mass Added
[b]M1, M2, M3 masses were added Represents Specimen with Added Mass 1, Added Mas 2 and Added Mass 3. For M1 only one mass was added, for M2 two masses were added, for M3 three

Table 4.3. Solutions for values of K_{metal} and J_o as obtained from the drive plate calibration for UofA Device 2 (modified from Deschenes, 2015).

Calibration rods	Compared Masses		Average Resonant Frequency	Momenet of Inertia	Torsional stiffness	Average Torsional stiffness
	Series 1	Series 2	F_m Ave Hz	J_o $kg{\cdot}m^2$	K_{metal} N·m/rad	Ave K_{metal} N·m/rad
1 31- Hz	NM	M1	32.28	2.870E-03	**122.10**	**122.98**
	NM	M1&2	32.79	2.811E-03	**122.98**	
	NM	M1,2,3	31.35	2.789E-03	120.08	
	M1	M1&2	**31.28**	**2.766E-03**	**123.86**	
	M1	M1,2,3	**30.84**	**2.752E-03**	119.11	
	M2	M1,2,3	**30.36**	**2.737E-03**	114.79	
2 85-Hz	NM	M1	88.08	3.187E-03	1433.65	**892.61**
	NM	M1&2	86.78	2.998E-03	1115.42	
	NM	M1,2,3	85.59	2.933E-03	**950.41**	
	M1	M1&2	**85.52**	**2.809E-03**	**912.81**	
	M1	M1,2,3	**84.33**	**2.799E-03**	**814.61**	
	M2	M1,2,3	**83.03**	**2.788E-03**	737.03	
3 120-Hz	NM	M1	125.16	2.800E-03	1707.63	**1673.32**
	NM	M1&2	123.33	3.286E-03	**1890.00**	
	NM	M1,2,3	121.70	3.174E-03	**1507.77**	
	M1	M1&2	**121.83**	**2.838E-03**	2620.15	
	M1	M1,2,3	**120.20**	**2.883E-03**	**1622.19**	
	M2	M1,2,3	**118.37**	**2.935E-03**	1080.23	

*The bold data were used to determine the average value and make a plot of moment of inertia as a function of resonant frequency

The K_{metal} value was also be verified by utilizing Equation 4.1.

$$G = \frac{K_{metal} L}{J} \qquad \text{(Equation 4.1)}$$

Where:

G = torsional shear modulus of aluminum calibration specimen (G=24 GPa),

L = length of the calibration specimen (m), and

J = polar moment of inertia (m^4) ($J = \frac{\pi D^4}{32}$ where D is the diameter of the calibration specimen shaft).

The drive plate mass polar moment of inertia values, as a function of frequency, that were obtained for two devices at the University of Arkansas are presented in Figure 4.2. The UofA results were also compared with the J_o calibration results obtained from the following entities: Utah State University [USU], the University of Texas [UT], the University of Southampton [US], Rensselaer Polytechnic Institute [RPI], the University of Colorado [CU] and Kleinfelder. The reference values presented in Figure 4.2 were obtained from Sasanakul (2005), Clayton et al. (2009), Kasantikul (2009), Khosravi (2013), and Laird (2013).

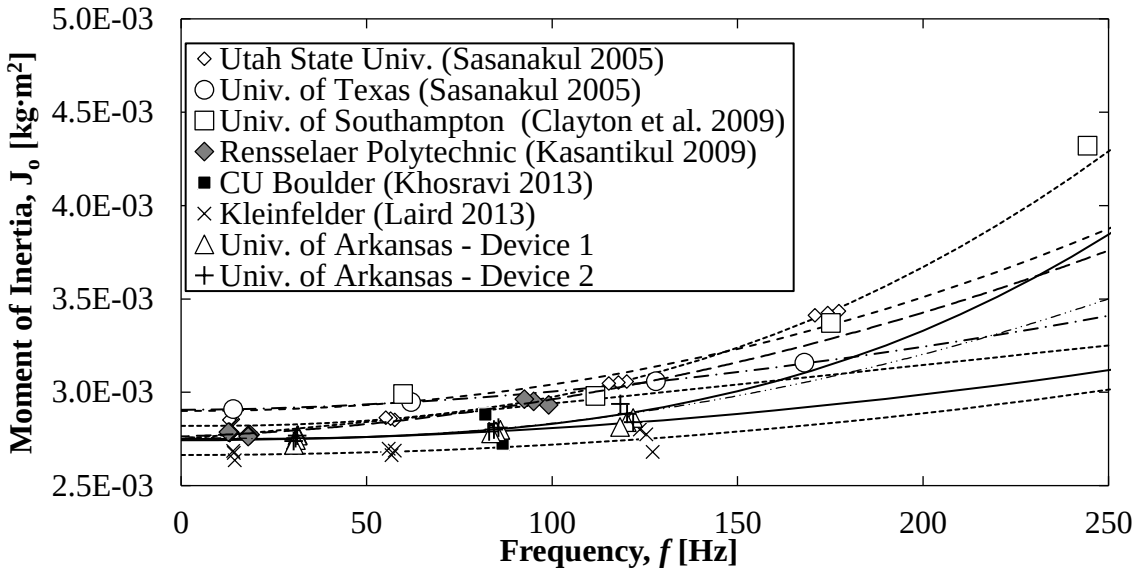

Figure 4.2. Drive plate mass polar moment of inertia (Jo) as a function of frequency (from Deschenes, 2015).

The power functions that were used to determine the frequency dependency on the experimentally determined J_o values from UA RCTS Devices 1 and 2 are shown as below:

$J_o = 0.002743 + 9.7408 \times 10^{-9} \overline{f_{i,j}}^{1.912}$ (J_o calibration for UA RCTS Device 1)

$J_o = 0.002750 + 1.6513 \times 10^{-10} \overline{f_{i,j}}^{2.8447}$ (J_o calibration for UA RCTS Device 2)

The J_0 value for the UA RCTS Device 1 was numerically smaller than the J_0 values that were found by Sasanakul (2005), Clayton et al. (2009), and Kasantikul (2009) for the respective drive plate assemblies located at USU, UT, US, and RPI. The values of the at rest mass polar moment of inertia for the drive plates of the UA RCTS Device 2 and the RPI device were found to be equal ($2.750 \cdot 10^{-3}$ kg·m2). The UA J_0 values and the experimentally determined calibration functions were found to closely match the unpublished Kleinfelder calibration curve (Laird 2013). The close correlation between the UA and Kleinfelder calibration functions was anticipated due to the fact that the Kleinfelder apparatus and both of the UA apparatuses were of the same make and model and were therefore expected to have similar physical properties (Deschenes, 2015).

4.3. Proximeter Calibration Factor, Kp (rad/V or degree/V)

4.3.1. Linear Proximeter Calibration

For the linear calibration of the proximeters, the output voltage of each of the proximeters was recorded at 0.127 mm (0.005 in.) intervals or 0.254 mm (0.01 in.) intervals as the tips of proximity probes moved toward or away from the proximeter target, respectively. The recorded change in the voltage that was measured during the corresponding proximeter displacement is shown in Table 4.4. The calibration factor of the proximeter system, K_p, was determined as the slope of the change in the output voltage (plotted on the y-axis) and the corresponding measured

gap between proximeter target and proximity probe tip (plotted on the x-axis). As shown in Figure 4.3, the calibration factor for UofA RCTS apparatus was the average of the slope values for the linear trendlines that were obtained from the right and left data points.

Table 4.4. The proximeter voltage change as a function of the proximeter displacement.

Displacement (mm)	Left Voltage	Left Voltage Change	Right Voltage	Right Voltage Change
	[V]	[V]	[V]	[V]
0	-0.50	0	-0.48	0
0.254	-1.21	-0.70	-0.50	-0.02
0.508	-3.32	-2.82	-1.13	-0.65
0.762	-5.48	-4.98	-3.22	-2.74
1.016	-7.74	-7.23	-5.38	-4.89
1.27	-9.99	-9.49	-7.63	-7.14
1.524	-12.34	-11.84	-9.88	-9.39
1.778	-14.76	-14.25	-12.19	-11.71

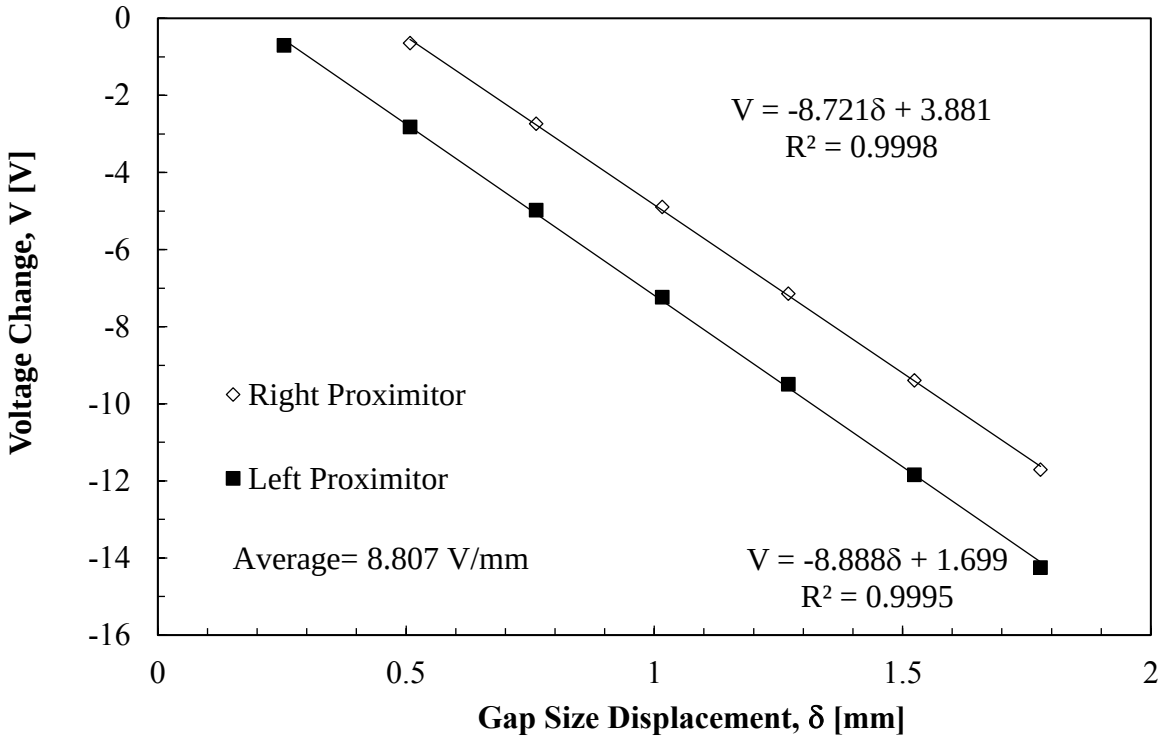

Figure 4.3. Plot of proximeter voltage change as a function of gap size displacement for the left and right proximeter as performed on UofA RCTS Device 2.

The aforementioned slope value was also inverted to produce a value of 0.114 mm/V. In a similar fashion to Scheer (1992), the inverted value was then divided by a value of two (2) to account for the use of two probes together to procedure a value of 0.057 mm/V (displacement). The displacement value (0.057 mm/V) was converted to rotational units by dividing the obtained value by the radius from the center of rotation to the center of the tip of each proximity probe. A distance of 20.24 mm center-to-center was used for the two UofA devices, as shown in Figure 4.4. The rotation angle is typically very small, so the use of the arctangent does not typically change the calibration factor results but was used for completeness. The final value of the proximeter calibration factor, K_P, by means of the linear displacement method for Device 2 at the UofA was determined to be **0.0028 rad/V.**

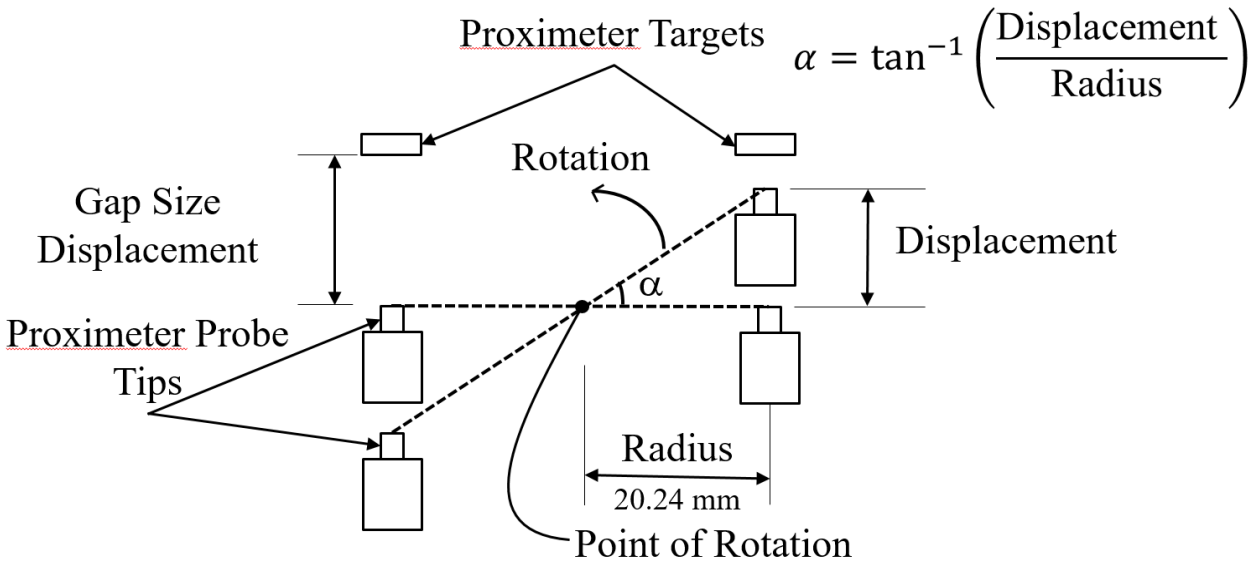

Figure 4.4. A schematic to convert the proximeter displacement unit to rotation unit.

4.3.2. Rotational Proximeter Calibration

During the rotational calibration of the proximeter, the voltage change was recorded, at 0.35 degree intervals or 0.7 degree intervals, as the proximity probe tips moved toward or away

from the proximeter target respectively. Each proximeter voltage change that was measured for the corresponding proximeter rotation angle is presented in Table 4.5. The calibration factor of the proximeter system, K_p, was determined to be the slope of the linear trendline through the data points that are shown in Figure 4.5.

Table 4.5. Proximeter voltage change as a function of the proximeter rotation angle.

Proximeter Voltage Change ΔV	Proximeter Rotation Angle α
[V]	[degree]
19.5	1.406
14.311	2.109
9.122	2.813
5.551	3.516
1.98	4.219

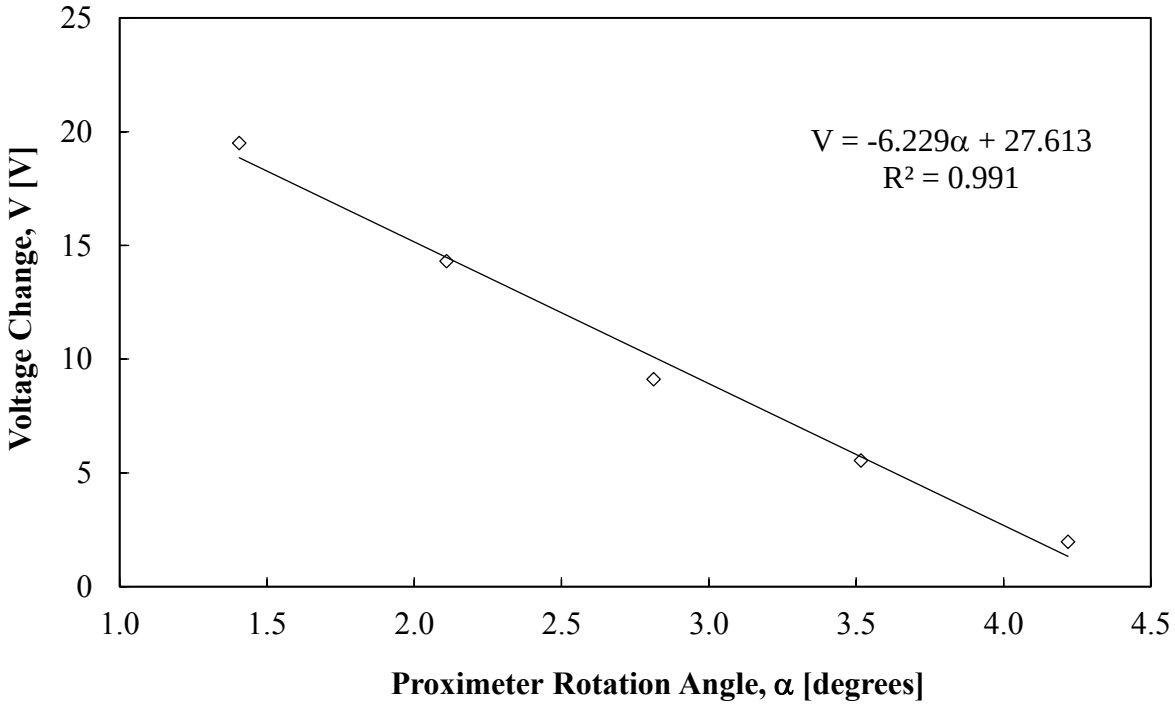

Figure 4.5. Plot of proximeter voltage change as a function of proximeter rotation angle for the left and right proximeter as performed on UofA RCTS Device 2.

From Figure 4.5, the average proximeter calibration was 6.2293 V/Degree which is equal to **0.0028 rad/V.** Therefore, the results between two different methods were with in good agreement with only 0.12 percent difference between the linear calibration and the rotational calibration. A detail calculation of K_P, using the data collected at the UofA, is provided in Appendix A- Section 2.

4.4. The Torque Calibration Factor, K_T (N.m/V)

The torque calibration factor was calculated using the aforementioned candlestick calibration specimens that each had known geometries and known material properties. Torsional Shear (TS) tests were performed on the three different calibration rods that included the thin rod, the middle rod and the thick rod with diameters of 0.375 inches, 0.5625 inches, and 0.75 inches, respectively. The TS tests were performed at frequency values of 0.1Hz, 0.5Hz, 1Hz and 2Hz. During the torque factor calibration, the drive coil was driven with the following amounts of supplied voltage: 30mV, 75mV, 150mV, 300mV, 600mV, 1200mV, 2400mV, and 3000mV. Corresponding values for the maximum coil excitation, V_T, and the maximum proximeter difference, V_P, for the three calibration specimens are shown in Figure 4.6. With the known value of K_{metal}, that was obtained from the procedure and described in Section 4.1 and a measured ratio of V_P/V_T, the torque calibration factor was calculated using the Equation 3.4, as previously presented.

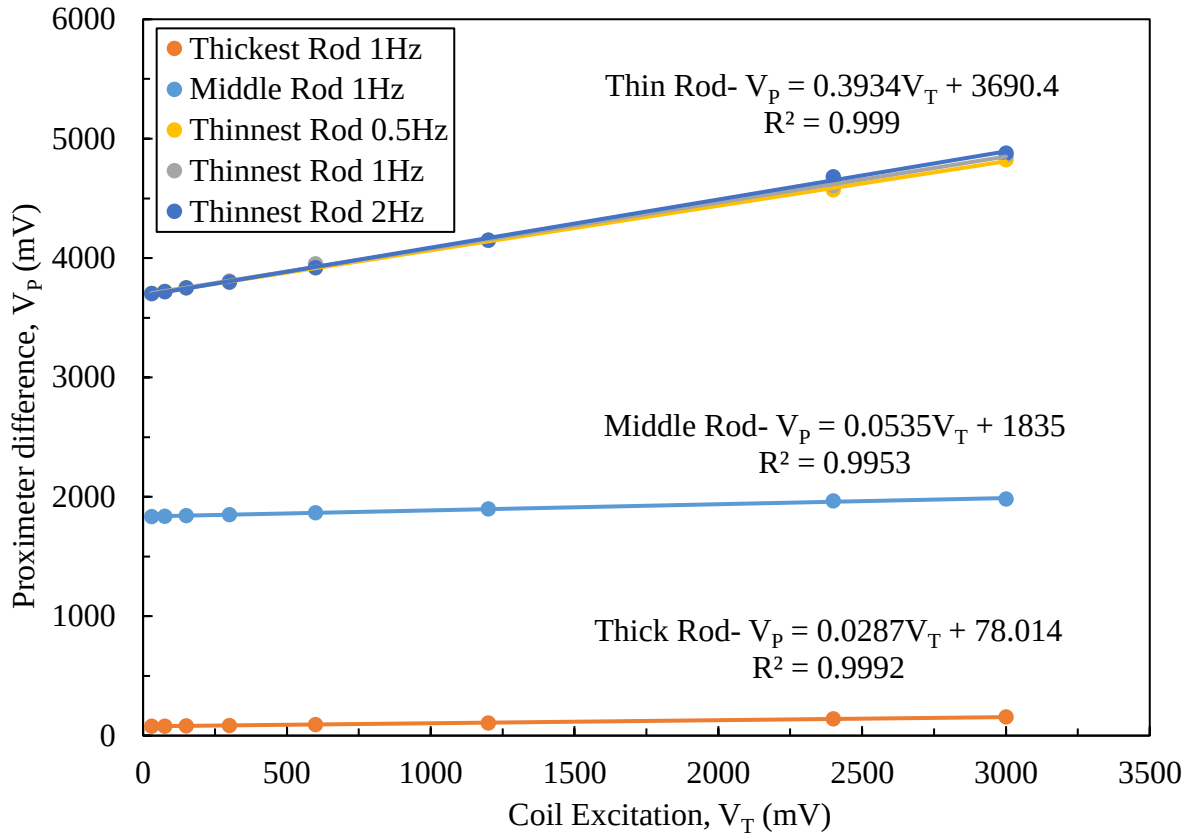

Figure 4.6. Plot of maximum proximeter difference as a function of coil excitation for the three calibration rods performed using the UofA RCTS Device 2.

The torque calibration factors, K_T for the thinnest, the middle and the thickest calibration specimen are 0.1357, 0.1339, and 0.1347 N·m/V, respectively. By taking the average of these values, the final value of K_T was determined to be **0.1347 N·m/V.** An example calculation for the determination of K_T, using the data collected at the UofA, is provided in Appendix A- Section 3.

4.5. Conclusions

By following the proposed standar, as presented in Chapter 3, the mass polar moment of inertia values, J_o, for the UofA and NGI drive plates in the UofA and NGI RCTS devices were similar to but smaller than to J_o values found in other devices at Utah State University (USU), the University of Texas (UT), the University of Southampton (US), and Rensselaer Polytechnic

Institute (RPI). The obtained J_o values for the UofA devices closely matched the J_o values for the Klienfelder device.

Likewise, by following the proposed ASTM Standard that was presented in Chapter 3, calibration factors were determined for the proximeter and drive coil (torque). The proximeter calibration factor, K_P, was determined to be valid because the obtained results were consistent for the linear and the rotational calibration method (0.0028 rad/V). The torque calibration factor, K_T, was also determined to be valid. The torque calibration factor was determined to be 0.1347 N·m/V.

CHAPTER 5: RESULTS AND DISCUSSION RELATED TO THE RCTS TESTS THAT WERE PERFORMED ON OTTAWA SAND

5.1. Chapter Overview

RCTS test results from tests performed on Ottawa Sand, with an applied isotropic confining pressure, are presented in this chapter. These tests were conducted by using the Stokoe-type Resonant Column Torsional Shear (RCTS) devices at the University of Arkansas (UofA) after the devices were properly calibrated. All tests were performed in accordance with the proposed ASTM procedures that were previously provided in Chapter 3.

5.2. RCTS Test Results from Tests on Ottawa Sand

RCTS were conducted on Ottawa Sand specimens with an initial void ratio of 0.617 (as obtained by assuming that the specific gravity of the Ottawa Sand was 2.65). The tests were sequentially perform while the confining pressure increased from 26.5 kPa to 50 kPa to 71 kPa. The RC tests were performed by initially driving the excitation coils with low excitation voltage (0.5 mV). After the initial driving, the excitation voltage gradually increased (1 mV, 3 mV, 6 mV, 12 mV, 20 mV, 35 mV, 50 mV, 75 mV and 100 mV) for subsequent tests at each confining pressure. A small-strain amplitude check was conducted after each large strain increment to account for the change in the maximum shear modulus after driving the coils with higher amounts of excitation voltage. The results of the RC tests on Ottawa Sand at the three isotropic confining pressure of 26.5 kPa, 50 kPa and 71 kPa are shown in Figure 5.1 and Figure 5.2. It can be seen that the shear modulus increased as the confining pressure increased. In addition, the shear modulus decreased with an increase in shear strain.

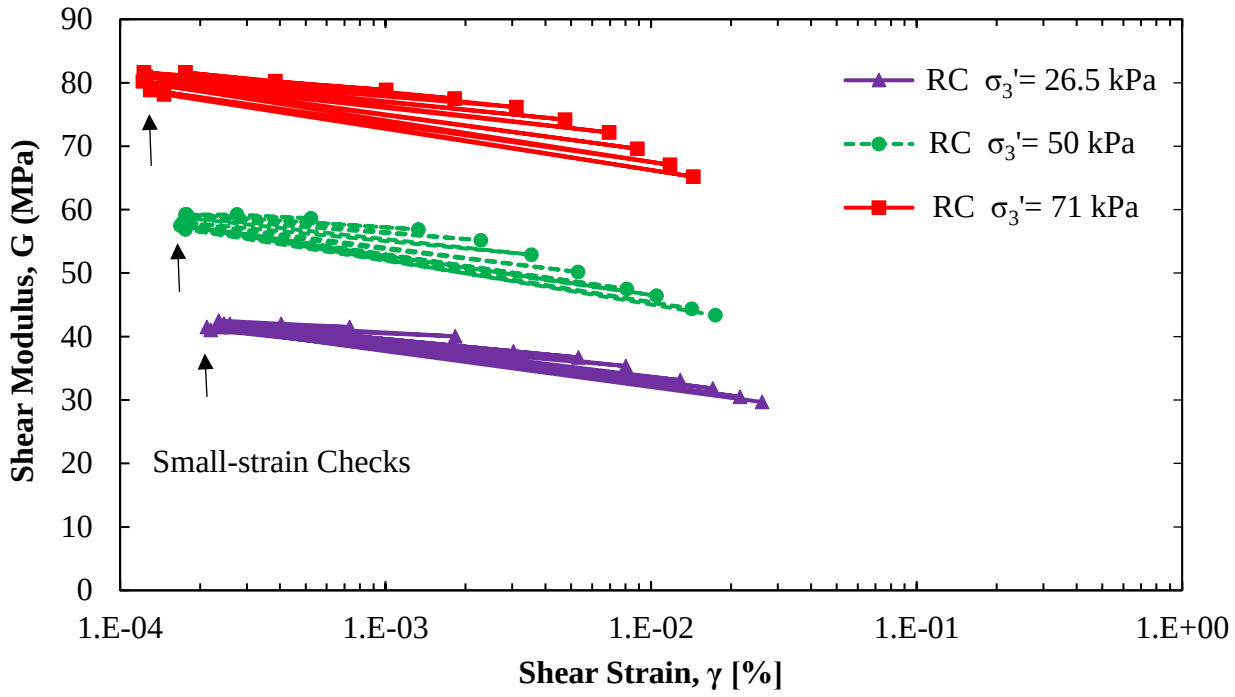

Figure 5.1. Plot of shear modulus as a function of shear strain for a medium-dense Ottawa Sand specimen at isotropic confining stresses of 26.5, 50 and 71 kPa as performed in the UofA RC Device (small-strain checks are also shown for completeness).

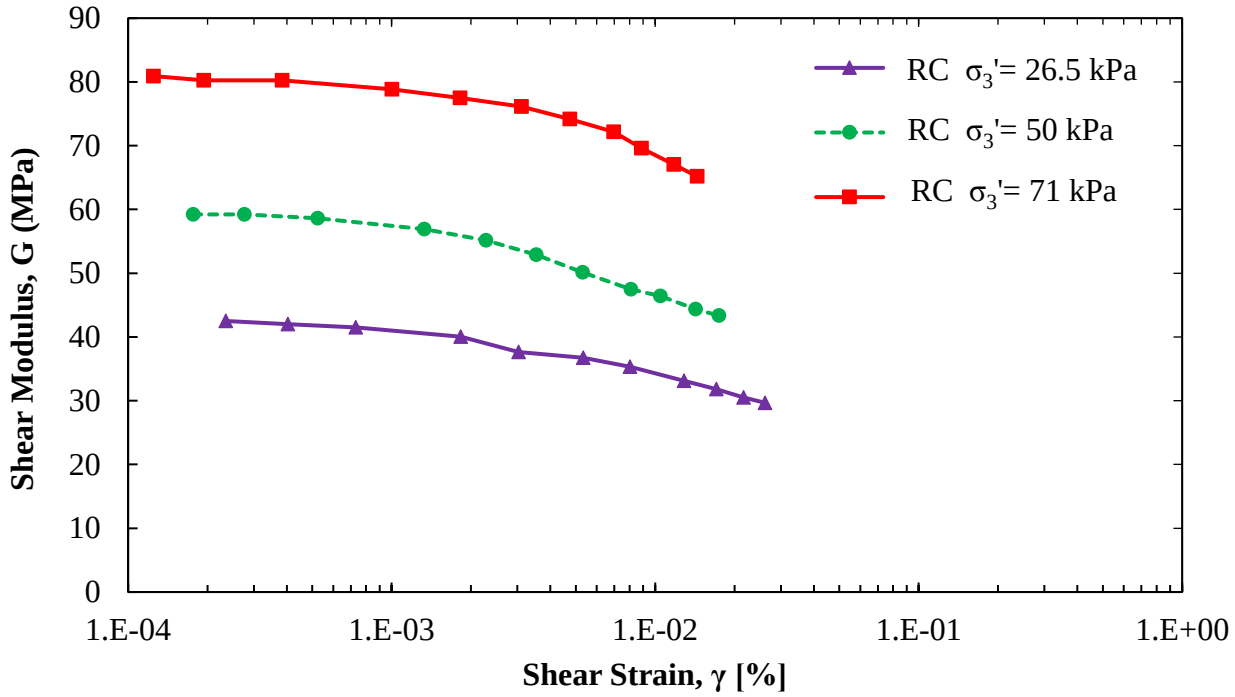

Figure 5.2. Plot of shear modulus as a function of shear strain for a medium-dense Ottawa Sand specimen at isotropic confining stresses of 26.5, 50 and 71 kPa as performed in the UofA RC Device (without showing small-strain checks).

One small-strain TS test with low excitation voltage (10 mV) was performed after one small-strain RC test (0.5 mV) to measure the maximum shear modulus. After 1) one TS small-strain test was performed by using a low excitation voltage and after the subsequent RC tests, the remainder of the TS test was performed with the excitation voltage values of 300 mV, 500 mV, 800 mV, 1200 mV, 1600 mV, 2000 mV, 2400 mV, 2800 mV, 3200 mV, 3600 mV and 4000 mV.

By performing the full RCTS test, the modulus reduction curve and the damping curve were collected for each confining stress. The modulus reduction curve and the damping curve for a medium-dense Ottawa Sand specimen at a confining pressure of 71 kPa, as performed at the University of Arkansas, are shown in Figure 5.3 and Figure 5.4, respectively. It can be seen that there is a good agreement between the RC and the TS results. These measured curves were also compared Darendelli (2001) curves. As shown in Figure 5.3, the modulus reduction curve was typically located above the modulus reduction curve obtained from Darendelli (2001). The damping curve that was obtained by performing the tests in the UofA apparatus was also predominantly above the Darendelli (2001) curve as shown in Figure 5.4. While the RC damping values had a good agreement with Darendelli (2001) model, the TS damping values did not follow the same trend as the Darendeli (2001) model for shear strain values greater than $2x10^{-2}$ percent. The combined RCTS modulus reduction and damping curves that were measured at three different confining pressures are presented in Figure 5.5 and Figure 5.6, respectively. Modulus reduction curves obtained at higher confining pressures were located above and to the right of curves obtained at lower confining pressures.

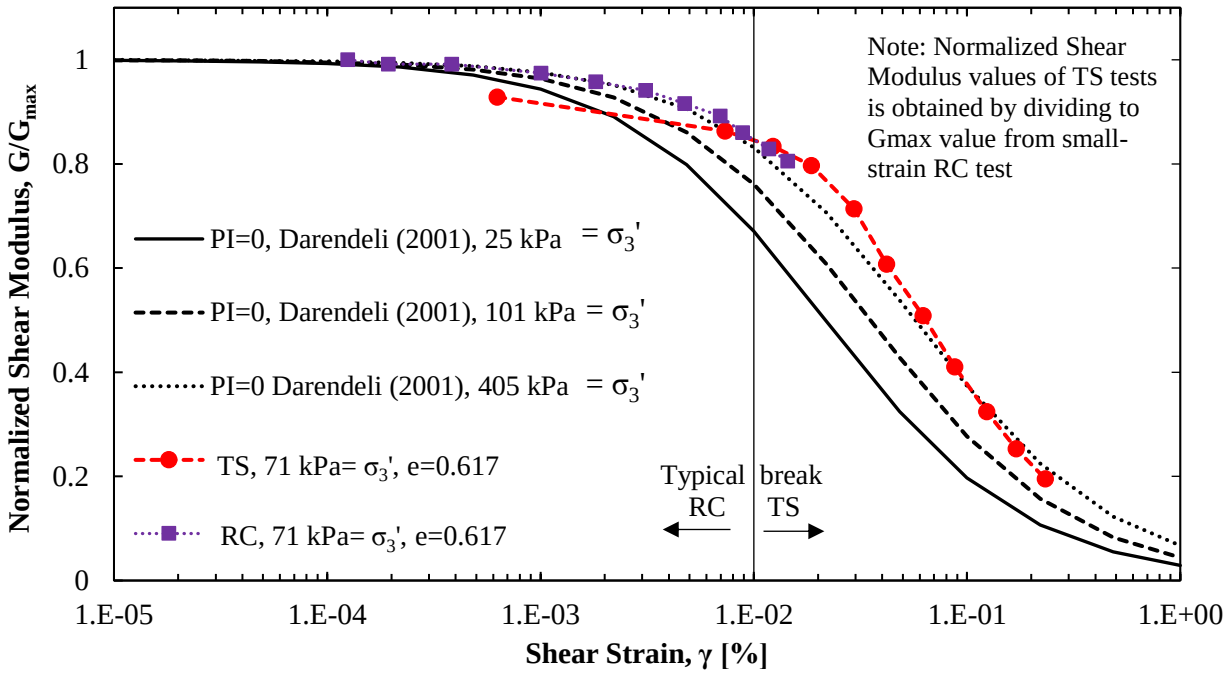

Figure 5.3. Modulus reduction curve for Ottawa Sand at a confining pressure of 71 kPa and void ratio of 0.617 using the UofA Device 2.

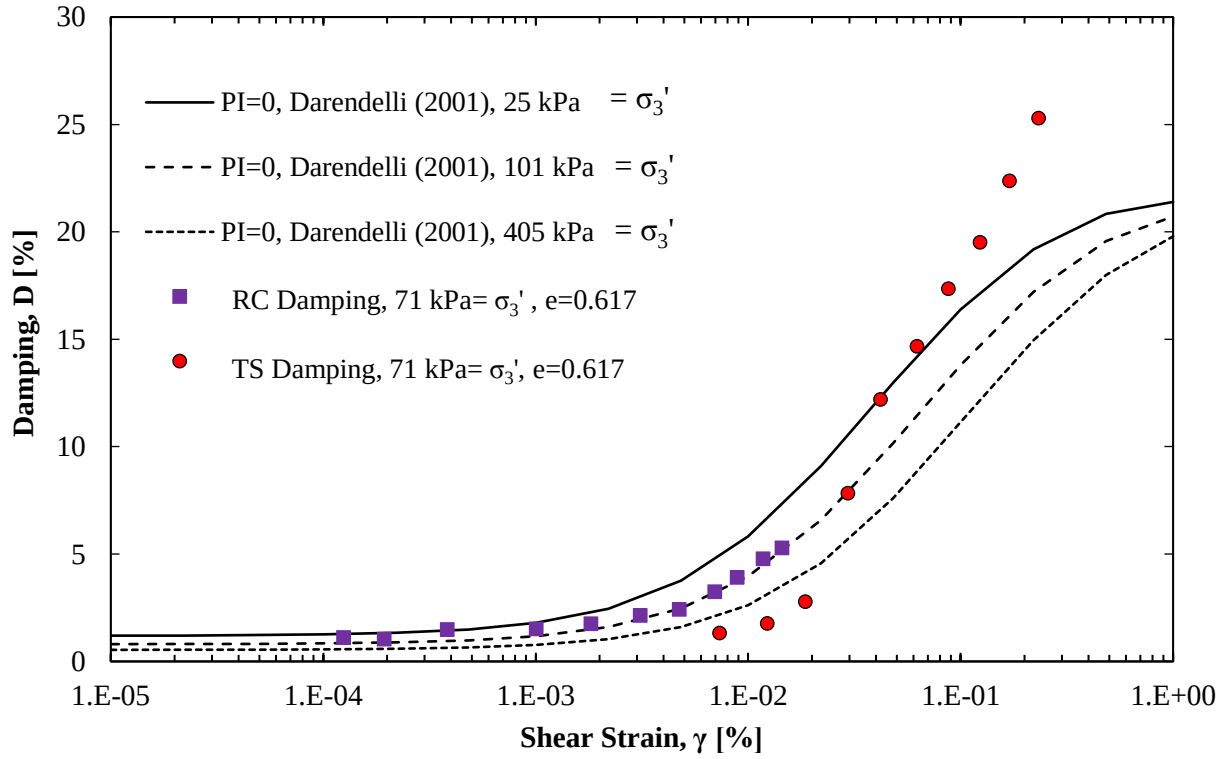

Figure 5.4. Damping curve for Ottawa Sand at a confining pressure of 71 kPa and void ratio of 0.617 using the UofA Device 2.

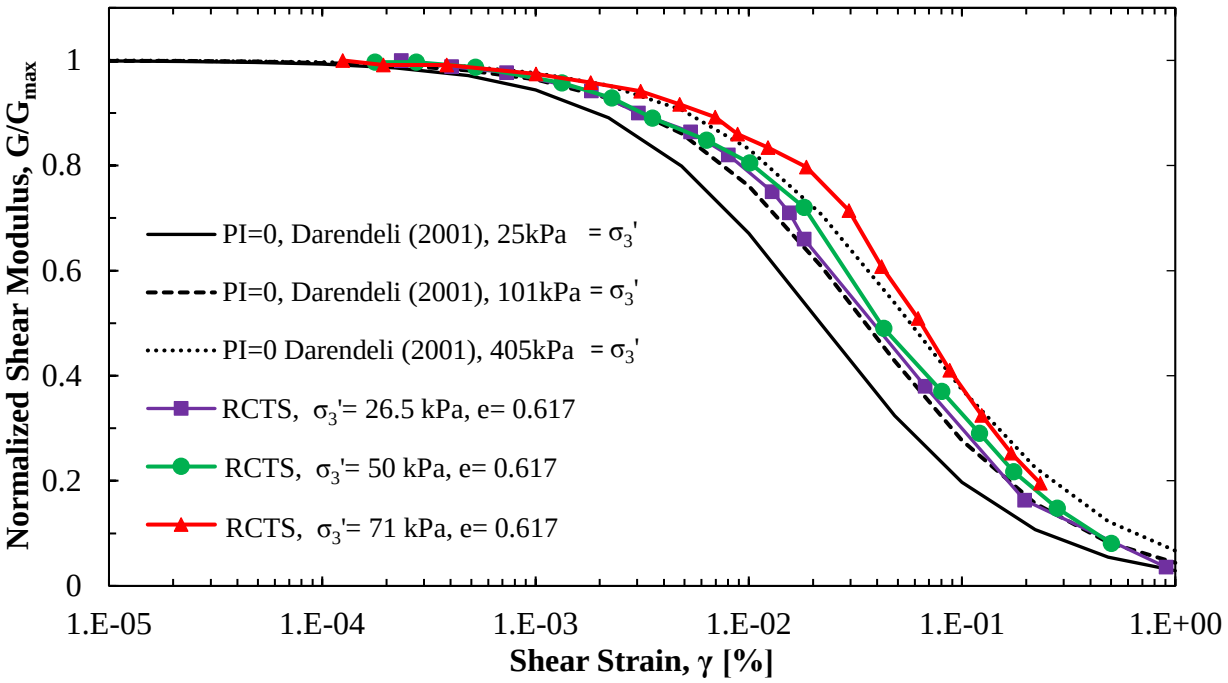

Figure 5.5. Plot of RCTS modulus reduction curve for Ottawa Sand at 26.5, 50, and 71 kPa isotropic confining pressure.

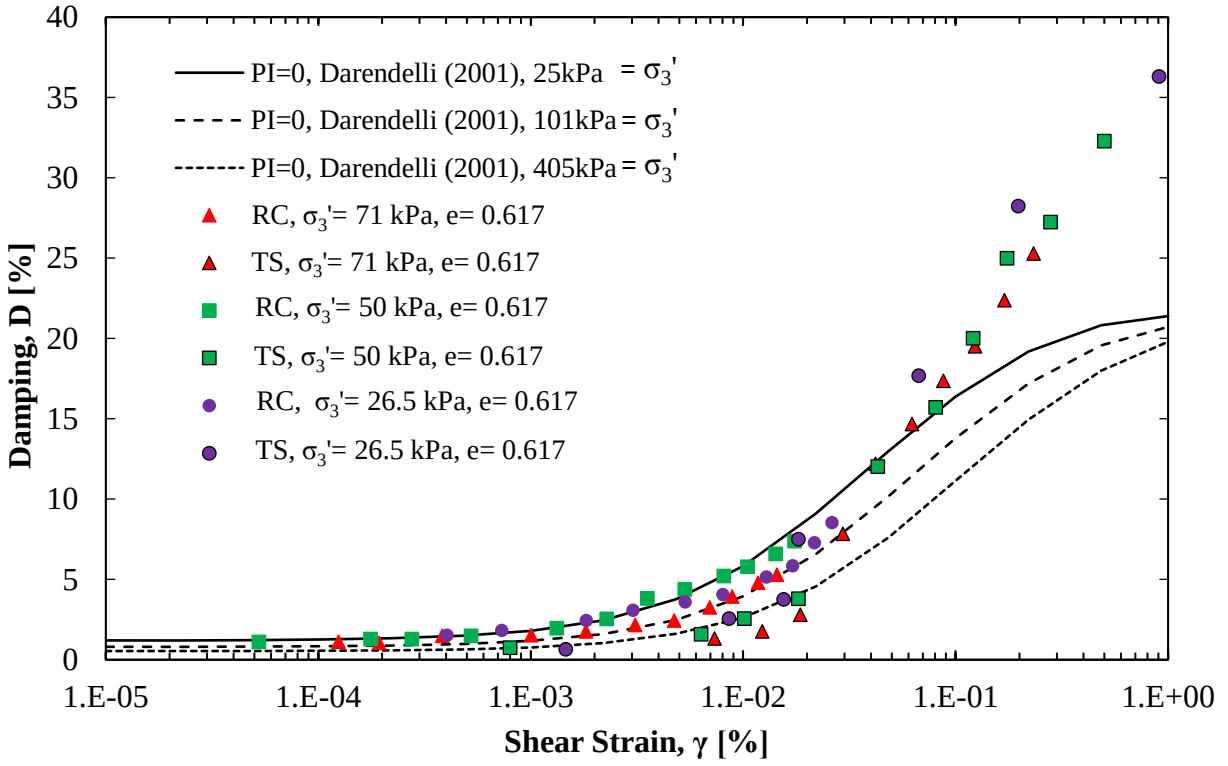

Figure 5.6. Plot of RCTS damping curve for Ottawa Sand at 26.5, 50 and 71 kPa isotropic confining pressure.

5.3. Correction of Modulus Reduction Curve for TS Results

In addition to the results from the RCTS tests conducted on samples with a void ratio of 0.617, the results from RCTS tests that were conducted on a loose Ottawa Sand specimen with void ratio of 0.857 are presented herein. The shear modulus results, that were obtained from the TS portion of the test, were corrected by dividing the shear modulus values with the corresponding small-strain shear modulus that were collected during the small-strain RC check. The purpose of these checks was to correct the normalized TS results in the modulus reduction curve. It was found that it was better to perform a small-strain TS check to correct TS results rather than a small-strain RC check. However, the smallest TS check was performed at shear strain of 1.12×10^{-3} percent, where the soil properties were no longer in the elastic range. The small-strain RC check was selected to correct the TS results. The reason of using small-strain RC checks after each TS test was to correct for the change in the maximum shear modulus that developed while performing the larger strain TS tests. Normally, the maximum shear modulus value decreased from three (3) to seven (7) percent after performing the higher amplitude RC or TS tests. The normalized modulus reduction curve of the loose Ottawa Sand specimen, when subjected to a 75 kPa confining pressure, before and after performing the correction, are shown in Figure 5.7 and Figure 5.8, respectively. After the correction, the TS curve shifted upward, and the TS curve tied into RC test result data.

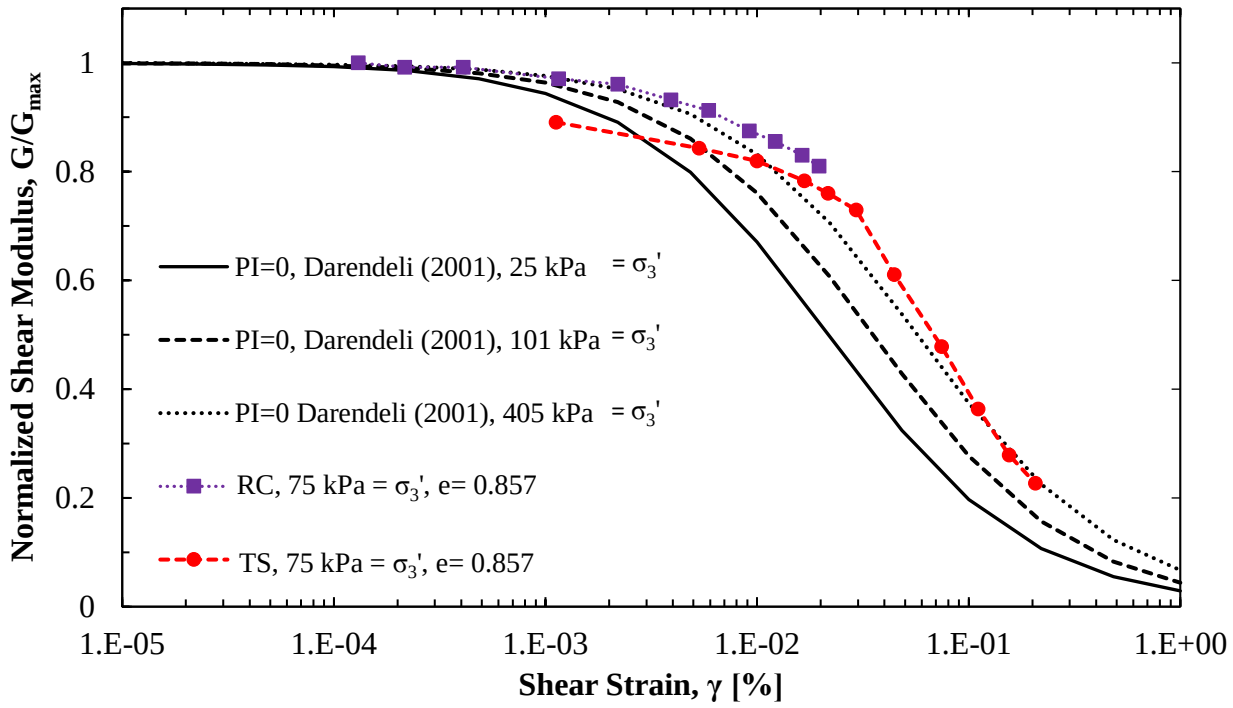

Figure 5.7. Plot of modulus reduction curve of loose Ottawa Sand (e=0.857) at 75 kPa confining pressure (before dividing the TS test results by the following up small-strain RC check).

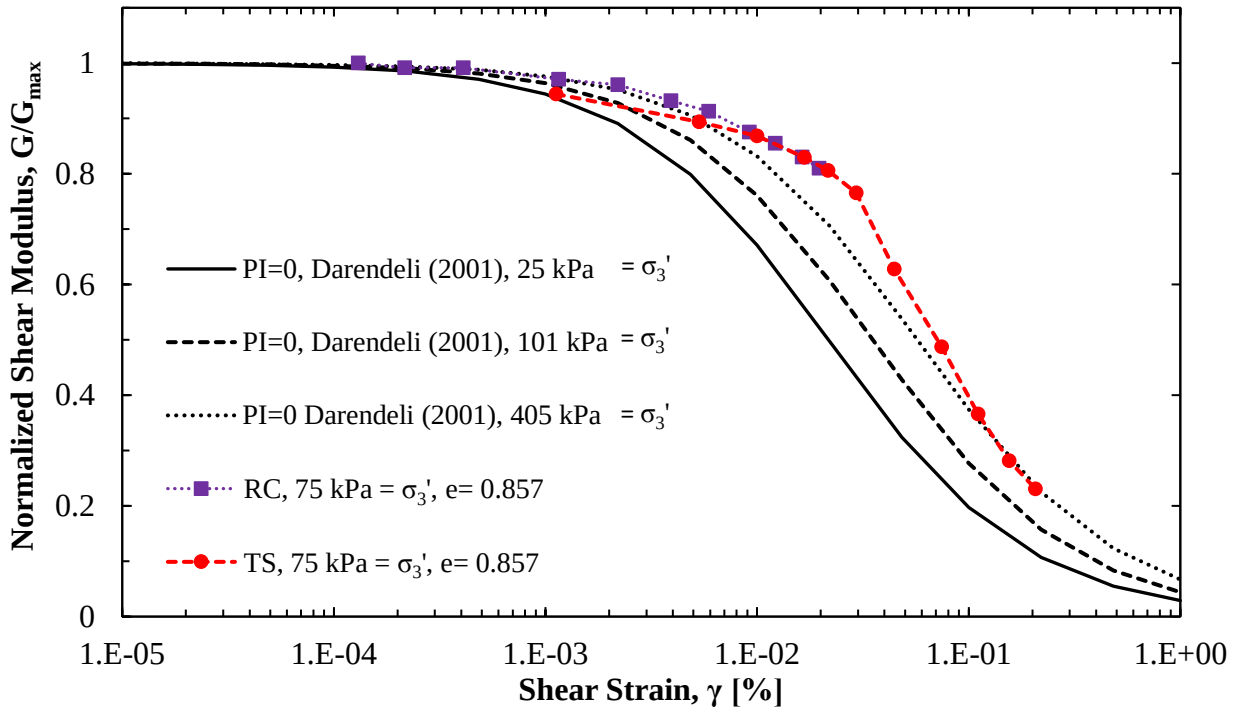

Figure 5.8. Plot of modulus reduction curve of loose Ottawa Sand (e=0.857) at 75 kPa confining pressure (after dividing the TS test results by the following up small-strain RC check).

5.4. Comparison of RC Test Results with Bender Element Test Results

The RC tests results from tests performed on Ottawa Sand with void ratio of 0.617, with a range of effective stresses from 41 kPa to 76 kPa, are presented in this section. As shown in Figure 5.9, the obtained measured shear wave velocity values from the RC tests were compared with shear wave velocity values obtained from bender element tests performed in a triaxial apparatus on an Ottawa Sand sample with average void ratio of 0.62. The bender element results were obtained from Salazar and Coffman (2014).

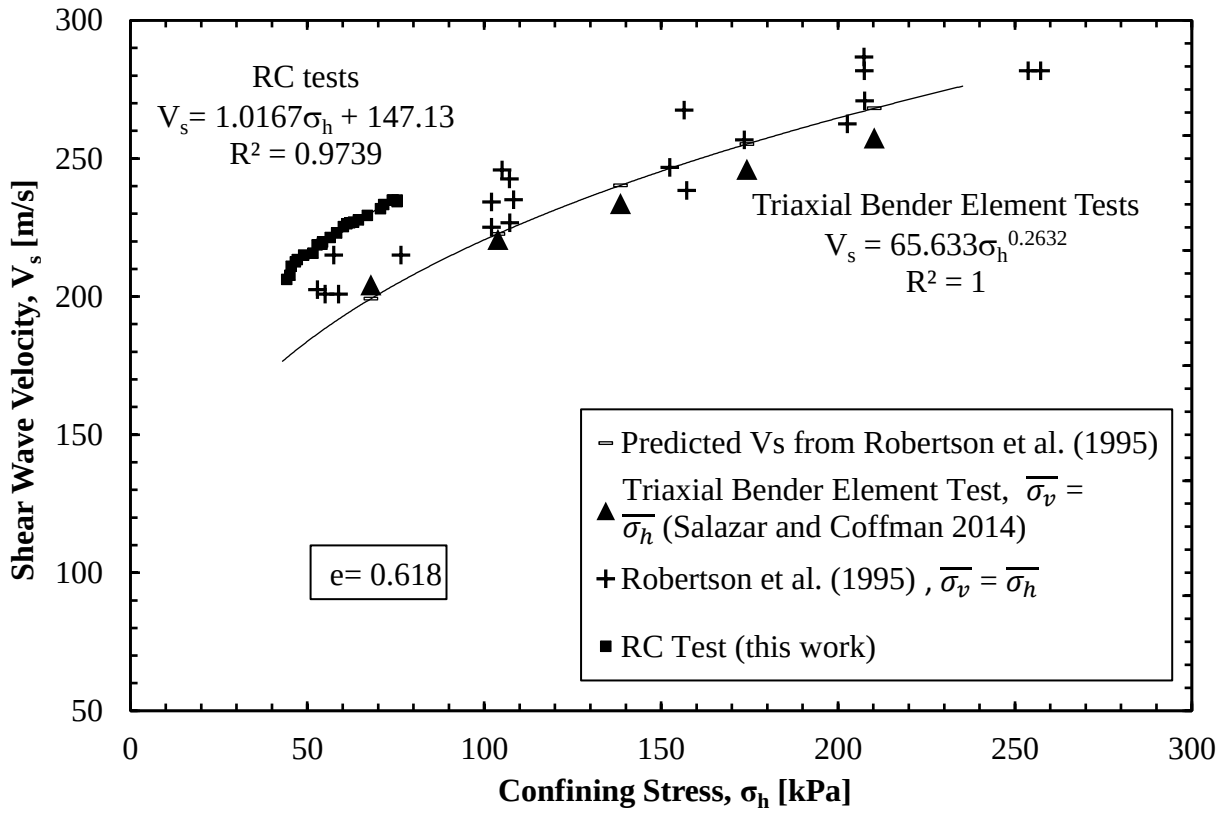

Figure 5.9. Predicted shear wave velocity of medium-dense, dry, Ottawa Sand as a function of confining stress and void ratio under isotropic stress conditions (modified from Salazar and Coffman, 2014).

From Figure 5.9, there is an obvious trend that shear wave velocity values from the RC tests were higher than those from the bender element test. To be more specific, shear wave velocity values from the RC tests were between 187 and 222 m/s for confining stress levels

ranging from 45 to 80 kPa. The shear wave velocity values that were obtained from the bender element test were between 178 and 208 m/s for confining stress levels ranging from 44 to 75 kPa. When compared with predicted results from Robertson et al. (1995), the shear wave velocity values from resonant column test and bender element test were found to be in good agreement, the difference between the results was only 5 percent. The difference might be attributed to the tests being performance on different devices and soil specimens.

5.5. Chapter Conclusions

Following the proposed ASTM standard that was presented in Chapter 3, RCTS test were performed on Ottawa Sand specimens using the Stokoe-type devices at the University of Arkansas. Modulus reduction curves and damping curves were compared with curves developed at the University of Texas. The UofA obtained modulus reduction curve was found to plot at higher values than the Texas' curves, but both curves follow the same trend. The UofA damping curves compared well with the Texas curves at shear strain levels less than 10^{-2} percent, but the UofA damping curves were above the Texas curves at shear strain levels greater than 10^{-2} percent.

The UofA obtained RCTS shear wave velocity values for the Ottawa Sand specimens also compared with results from bender element test performed on similar specimens, at the same confining pressure, that were also conducted at the UofA. Specifically, a five (5) percent difference in shear wave velocities was observed between the bender element obtained values (178 m/s) and the resonant column obtained values (187 m/s).

CHAPTER 6: CONCLUSIONS

6.1. Chapter Overview

The conclusions are presented herein in this chapter. In Section 6.2, the calibration for UofA devices are provided. The main findings of RCTS results performed on Ottawa Sand using UofA RCTS Device 2 are discussed in Section 6.3. Finally, recommendations are provided in Section 6.4.

6.2. Calibrations

By following the proposed standard to calibrate the RCTS Stokoe-type device, the mass polar moment of inertia value, J_o, for the UofA and NGI drive plates in the UofA and NGI RCTS devices were similar but smaller than to J_o values found other authors from Utah State University (USU), the University of Texas (UT), the University of Southampton (US), and Rensselaer Polytechnic Institute (RPI). The obtained J_o values for the UofA devices closely matched the J_o values for the Klienfelder device.

Calibration factors were determined for the proximeter and drive coil (torque). The proximeter calibration factor, K_P was determined to be valid because the obtained results were consistent for the linear and the rotational calibration method (0.0028 rad/V). The torque calibration factor, K_T was also determined to be valid. The torque calibration factor was determined to be 0.1347 N.m/V.

6.3. RCTS test Results performed on Ottawa Sand

Following the proposed ASTM standard, RCTS test were performed on Ottawa Sand specimens using the Stokoe-type devices at the University of Arkansas. Modulus reduction curves and damping curves were compared with curves developed at the University of Texas.

The UofA obtained modulus reduction curve was found to plot at higher values than the Texas's curves, but both curves follow the same trend. The damping curves compared well with the Texas curves at the shear strain levels less than 10^{-2} percent, but the UofA damping curve was above the Texas curve at the shear strain levels greater than 10^{-2} percent. Shear wave velocity values for the Ottawa Sand specimens from the RCTS tests were also compared with results from bender element test performed on similar specimens at the same confining pressure. There is a good agreement in the results. 5 percent difference in shear wave velocities was observed between the bender element obtained values (178 m/s) and the resonant column obtained values (187 m/s).

6.4. Recommendations

A proposed RCTS standard test method was presented herein, but the specific test method should be selected based upon the specifics of the project. Testing methods should use the best and most up to date calibration factors because these calibration factors can cause the change in results significantly.

For the UofA RCTS devices, it is recommended to replace an existing proximeter system by a micro-proximeter system which has higher resolution. With this renovation, the small-strain value of TS test, which less than 10^{-4} percent, can be determined and compared with the small-strain value of RC test.

REFERENCES

ASTM D1587/D1587M-15 Standard Practice for Thin-Walled Tube Sampling of Fine-Grained Soils for Geotechnical Purposes, West Conshohocken, PA, 2015, https://doi.org/10.1520/D1587_D1587M-15

ASTM D2216-10, Standard Test Methods for Laboratory Determination of Water (Moisture) Content of Soil and Rock by Mass, ASTM International, West Conshohocken, PA, 2010, www.astm.org

ASTM D3999/D3999M-11e1 Standard Test Methods for the Determination of the Modulus and Damping Properties of Soils Using the Cyclic Triaxial Apparatus, ASTM International, West Conshohocken, PA, 2011, https://doi.org/10.1520/D3999_D3999M

ASTM D4015-15e1 Standard Test Methods for Modulus and Damping of Soils by Fixed-Base Resonant Column Devices, ASTM International, West Conshohocken, PA, 2015, https://doi.org/10.1520/D4015-15E01.

ASTM D4220/D4220M-14 Standard Practices for Preserving and Transporting Soil Samples, ASTM International, West Conshohocken, PA, 2014, https://doi.org/10.1520/D4220_D4220M

ASTM D4767-11 Standard Test Method for Consolidated Undrained Triaxial Compression Test for Cohesive Soils, ASTM International, West Conshohocken, PA, 2011, https://doi.org/10.1520/D4767-11

ASTM D5311/D5311M-13 Standard Test Method for Load Controlled Cyclic Triaxial Strength of Soil, ASTM International, West Conshohocken, PA, 2013, https://doi.org/10.1520/D5311_D5311M

ASTM D7608-10 Standard Test Method for Torsional Ring Shear Test to Determine Drained Fully Softened Shear Strength and Nonlinear Strength Envelope of Cohesive Soils (Using Normally Consolidated Specimen) for Slopes with No Preexisting Shear Surfaces, ASTM International, West Conshohocken, PA, 2010, https://doi.org/10.1520/D7608-10

Blanchard, J.D. (2016). "Literature Review for Resonant Column Torsional Shear Test." CVEG 5113 Soil Dynamic, University of Arkansas, April 22, 2016.

Chen, A.T. F., and Stokoe, K. H., II (1979). "Interpretation of strain dependent modulus and damping from torsional soil tests." Rep. No. USGS-GD-79-002, NTIS No. PB-298479, U.S. Geological Survey, 46.

Clayton, C., Priest, J., Bui, M., Zervos, A., Kim, S., (2009). "The Stokoe Resonant Column Apparatus: Effects of Stiffness, Mass, and Specimen Fixity." Geotechnique, Vol. 59, No. 5, pp. 429-437.

Darendeli, Mehmet B., (2001). “Development of a New Family of Normalized Modulus Redction and Material Damping Curves”. Doctoral Dissertation. University of Texas at Austin. 395 pgs.

Deschenes, M.R., (2015). “Drive Plate Mass Polar Moment of Inertia in Stokoeo Type Resonant Column Devices”. Undergraduate Honors Theses, University of Arkansas.

Hardin, B.O. and Richart, F.E, Jr., (1963), “Elastic Wave Velocities in Granular Soils,” Journal of Soil Mechanics and Foundations Division, ASCE, Vol.89, No. SM1, Feb., pp.33-65.

Hardin, B.O and Music, J. (1965), “Apparatus for Vibration of Soil Specimens During the Triaxial Test,” Symposium on Instrumentation and Apparatus for Soils and Rocks, ASTM STP 392, ASTM, pp. 55-74.

Hwang, Seon Keun, (1997). “Dynamic Properties of Natural Soils.” Doctoral Dissertation. University of Texas at Austin.

Iida, K. (1938), “The Velocity of Elastic Waves in Sand,” Bulletin of the Earthquake Research Institute, Tokyo Imperial University, Vol. 16, pp. 131-144.

Iida, K. (1940), “On the Elastic Properties of Soil Particularly in Relation to Its Water Content,” Bulletin of the Earthquake Research Institute, Tokyo Imperial University, Vol. 18, pp. 675-690.

Isenhower, W.M., Stokoe, K.H., II, and Allen, J.C. (1987), “Instrumentation for Torsional Shear/ Resonant Column Measurements Under Anisotropic Stresses,” Geotechnical Testing Journal, GTJODJ, Vol. 10, No.4 Dec. pp. 183-191.

Kim, Dong-Soo, (1991). “Deformational Characteristics of Soils at Small to Intermediate Strains from Cyclic Tests”. Doctoral Dissertation. University of Texas at Austin.

Kasantikul, P., (2009). “Resonant Column and Torsional Shear Testing to Evaluate Soil Properties Deposited Using Dry Pluviation and Hydraulic Fill.” Masters Thesis. Rensselaer Polytechnic Institute, May, 191 pgs.

Keene, A.K., (2017).”Next-Generation Equipment and Procedures for Combined Resonant Column and Torsional Shear Testing”. Doctoral Dissertation. University of Texas at Austin.

Khosravi, Ali, (2011). “Small-strain Shear Modulus of Unsaturated, Compacted Soils During Hydraulic Hysteresis.” Doctoral Dissertation. University of Colorado, May, 170 pgs.

Laird, Joseph, (2013). “RE: Resonant Column Calibration.” Personal Electronic Mail Communication with Richard A. Coffman.

Kramer, S. L. (2014). Geotechnical earthquake engineering. Harlow, Essex: Pearson Education Limited.

Menq, F.Y. (2003). *Dynamic Properties of Sandy and Gravelly Soils*. PhD Dissertation, Department of Civil, Arcitectural and Environmental Engineering, University of Texas, Austin.

Ni, S.H. (1987), "Dynamic Properties of Sand Under True Triaxial Stress States from Resonant Column/ Torsional Shear Tests," PhD. Dissertation, the University of Texas at Austin, 421 pp.

Nuclear Regulatory Commission Nuclear Regulation CR-5739 (NRC NUREG CR-5739), (200). "Nuclear Regulation CR-5739 – Laboratory Investigation of Soils and Rocks for Engineering Analysis and Design of Nuclear Power Facilities". United States Nuclear Regulatory Commission. Prepared for the Division of Engineering Technology, Office of Nuclear Regulatory Research.

Richart, F.E. Jr., Hall, J.R. Jr., and Woods, R.D. (1970). Vibrations of Soils and Foundations. Prentice-Hall, Inc., Englewood Cliffs, New Jersey.

Salazar, S.E., Coffman, R.A., (2014). "Design and Fabrication of End Platens for Acquisition of Small-Strain Piezoelectric Measurements during Large-Strain Triaxial Extension and Triaxial Compression Testing." Geotechnical Testing Journal. Vol. 37, No.6, pp. 948-958.

Sasanakul, Inthuorn (2005). "Development of an Electromagnetic and Mechanical Model for a Resonant Column Torsional Shear Testing Device for Soils" Doctoral Dissertation, to the Department of Civil Engineering at Utah State University, 275 pgs.

Sasanakul, I., Bay, J., (2005). "Measurements of Nonlinear Dynamic Properties of Booneville Silty-Clays." Report for United States Geological Survey Award Number 04HQGR0055. 50 pgs.

Sasanakul, I., Bay, J., (2010). "Calibration of Equipment Damping in a Resonant Column and Torsonial Shear Testing Device." Geotechnical Testing Journal, Vol. 33, No. 5. Paper ID GTJ102475

Scheer, P. K. (1992), "Implementation Of A Resonant Column/Torsional Shear Testing Apparatus." Masters Thesis to the Department of Civil Engineering North Carolina State University, 229 pgs.

Trautwein Soil Testing Equipment, Co. (2008). "Calibration Rod 0.750 in." 6909 Ashcroft Rd Suite 104 Houston, TX 77081, 1 pg.

APPENDIX A

1. Drive plate mass polar moment of inertia, J_o:

Given: Example of the candlestick Sample 3.

Diameter of the candlestick Sample 3, d_r= 0.75 [in.] =19.05 [mm] (Table 4.1).

Diameter of the top plate of Sample 3, d_t= 1.375 [in.] = 34.93 [mm] (Table 4.1).

Height of the top plate of Sample 3, h_t= 0.5 [in.] = 12.7 [mm] (Figure 4.1).

Height of the candlestick Sample 3, h_r= 8 [in.] -0.5 [in.] – 0.5 [in.] = 7 [in.] = 177.8 [mm] (Figure 4.1).

Find: J_o and K_{metal}

Solution:

The volume of the top plate of Sample 3, $V_t = \pi \cdot h_t \cdot d_t^2/4 = \pi$ (12.7 mm) (34.93 mm)^2/4= 12170 [mm^3]= 1.217x10^{-5} [m^3].

The mass of the top plate of Sample 3, $m_t = \rho \cdot V_t$ = (2700 kg/m^3)(1.217x10^{-5} m^3)= 0.032859 [kg].

The polar mass moment of inertia of the top plate of Sample 3, $J_t = m_t \cdot d_t^2/8$= (0.032859 kg) (0.03493 m)^2/8= 5.011E-06 [kg·m^2].

Polar moment of inertia of the added mass number i, ΔJ_i [kg·m^2]= 1.853E-04 [kg·m^2] (Table 4.1).

$$K_{metal} = \frac{4\pi^2 \Delta J_i (f_r f_{r,i})^2}{(1-D^2)(f_r^{\,2} - f_{r,i}^{\,2})} = \frac{4\pi^2 (1.853\times10^{-4} kg\cdot m^2)(124.19Hz \times 120.280Hz)^2}{(1-0.00199^2)(124.19^2 - 120.280^2)Hz^2} = 1708[kg\cdot m^2]$$

$$J_o = \frac{\Delta J_i f_{r,i}^{\,2}}{f_r^{\,2} - f_{r,i}^{\,2}} - J_t = \frac{(1.853\times10^{-4} kg\cdot m^2)(120.28Hz)^2}{\left[(124.19Hz)^2 - (120.28Hz)^2\right]} - 5.011\times10^{-6}[kg\cdot m^2] = 2.80\times10^{-3}[kg\cdot m^2]$$

2. Proximeter calibration factor, K_P:

Given:

The average linear proximeter calibration factor, $K_{P,\ linear}$= 8.807 [V/mm].

Radius from the center of rotation to the center of the tip of each proximity probe, r= 20.24 [mm].

The average rotational proximeter calibration factor, $K_{P,\ rotational}$ = 6.2293 [V/degree].

Find: The proximeter calibration factor, K_P, in [rad/V]

Solution:

The displacement of a proximeter with accordance to the change in voltage=

$$\frac{1}{8.807[V/mm]} \times \frac{1}{2} = 0.057\ [mm/V]$$

The proximeter calibration factor, K_P, using the linear proximeter calibration method:

$$K_P = \tan^{-1}\left(\frac{Displacement}{Radius}\right) = \tan^{-1}\left(\frac{0.057mm/V}{20.24mm}\right) = 0.0028\ [rad/V]$$

The proximeter calibration factor, K_P, using the rotational proximeter calibration method:

$$K_P = \frac{1}{6.23[V/\deg]} \times \frac{\pi(rad)}{180(\deg)} = 0.0028\ [rad/V]$$

3. Torque calibration factor, K_T:

Given:

The proximeter calibration factor, K_P= 0.002805 [rad/V]

For the thin candlestick rod: the V_P/V_T value is 0.0287, and the K_{metal} value is 1673.32 [N·m/rad].

For the middle candlestick rod: the V_P/V_T value is 0.0535, and the K_{metal} value is 892.61 [N·m/rad].

For the thick candlestick rod: the V_P/V_T value is 0.3934, and the K_{metal} value is 122.98 [N·m/rad].

Find: Torque calibration factor, K_T:

Solution:

Using Equation 3.4, the torque calibration factor for the thin, middle and thick candlestick rod respectively are:

$$K_T = \frac{V_p}{V_T} K_p K_{metal} = (0.0287)(0.002805 rad/V)(1673.32 N \cdot m/rad) = 0.1347\ [N \cdot m/V]$$

$$K_T = \frac{V_p}{V_T} K_p K_{metal} = (0.0535)(0.002805 rad/V)(892.61 N \cdot m/rad) = 0.1340\ [N \cdot m/V]$$

$$K_T = \frac{V_p}{V_T} K_p K_{metal} = (0.3934)(0.002805 rad/V)(122.98 N \cdot m/rad) = 0.1357\ [N \cdot m/V]$$

By taking average of three calibration factor values, a calibration factor of 0.1348 [N·m/V] is used for further calculations.

4. RC test results:

Given: Ottawa Sand

The sample length, L= 0.06773 [m].

The sample mass, M=0.1259 [kg].

The sample diameter, D= 0.038 [m].

The specific gravity of Ottawa Sand, SG= 2.65.

The resonant frequency, f_r= 44.698 [Hz] or ω_r=280.846 [rad/s].

The selected amplitude= 0.4 [V].

$J_o = 0.002750 + 1.6513 \times 10^{-10} \overline{f_{i,j}}^{2.8447}$ (J_o calibration for UA RCTS Device 2)

The polar mass moment of inertia of the top plate, J_t= 5.011 x 10^{-6} [kg.m^2].

Find: Shear wave velocity, V_s, shear modulus, G and the damping, D.

Solution:

The mass polar moment of inertia of the soil specimen, J is found by solving Equation 3.6:

$$J = \frac{MD^2}{8} = \frac{(0.1259kg)(0.038m)^2}{8} = 2.27 \times 10^{-5} \ [kg \cdot m^2]$$

The drive plate mass polar moment of inertia, J_o for the UA RCTS Device 2:

$$J_o = 0.002750 + 1.6513 \times 10^{-10} (44.698)^{2.8447} = 2.758 \times 10^{-3} \ [kg \cdot m^2]$$

The shear wave velocity is found by solving Equation 3.7:

$$\frac{J}{J_o + J_t} - \frac{\omega L}{V_s}\tan\left(\frac{\omega L}{V_s}\right) = 0$$

$$\frac{2.27\times10^{-5}[kg\cdot m^2]}{2.758\times10^{-3}[kg\cdot m^2]+5.011\times10^{-6}[kg\cdot m^2]} - \frac{(280.846rad/s)(0.6773m)}{V_s}\tan\left[\frac{(280.846rad/s)(0.6773m)}{V_s}\right] = 0$$

$V_s = 209.862\ [m/s]$

The shear modulus of Ottawa Sand, G is calculated using Equation 3.8.

$$G = \rho V_s^2 = \frac{4M}{\pi D^2 L}V_s^2 = \frac{4\times0.1259kg}{\pi(0.038m)^2(0.06773m)}(209.862m/s)^2 = 72.18\ [MPa]$$

The damping ratio, δ, is calculated from Equation 3.9 using the half-power bandwidth method. The half-power bandwidth method is shown in Figure 7.1.

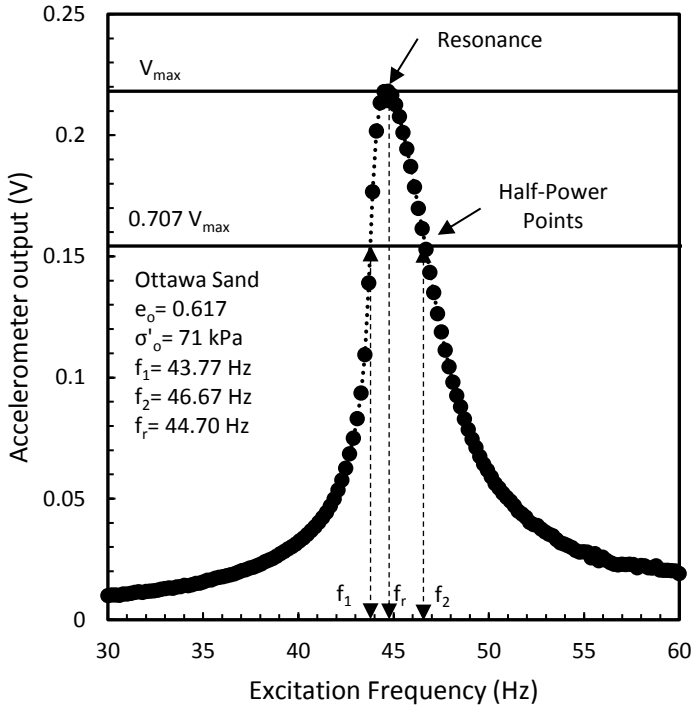

Figure 7.1. Half power bandwidth method using to calculate the damping ratio.

$$\delta = \frac{f_2 - f_1}{2f_r} = \frac{46.67Hz - 43.77Hz}{2(44.70Hz)}\times100\% = 3.24\ [\%]$$

5. RC shear strain calculation:

Given:

The acceleration of gravity, g= 9.81 [m/s^2].

The distance from the location of accelerometer to the center of specimen, r_a= 0.0508 [m].

The charge amplifier factor, CAF= 0.4 [g/V].

The conversion factor from RMS voltage to Single Amplitude voltage, CF= $\left(= \frac{\sqrt{2}}{(2\pi)^2} \right) = 0.03582$

The accelerometer output, a =0.21818 [V].

The resonant frequency, f_r= 44.698 Hz or ω_r=280.846 [rad/s].

The equivalent radius, ER= 0.82 for shearing strain less than 10^{-3} percent and 0.79 for shearing strain equals to 0.1 percent.

The sample length, L= 0.06773 [m].

The sample diameter, D= 0.038 [m].

Find: The shearing strain, γ

Solution:

$$\gamma = \frac{g}{r_a} \times CAF \times CF \times \frac{a \times D/2 \times ER}{L \times f_r^{\,2}} \times 100\%$$

$$\rightarrow \gamma = \frac{9.81\ m/s^2}{0.0508\ m} \times 0.4 g/V \times 0.03582 \times \frac{(0.21818V) \times (0.038m/2) \times 0.82}{0.06773m \times (44.698\ \text{Hz})^2} \times 100\% = 0.00695\ [\%]$$

6. TS test results:

The example calculation is at 0.5V amplitude TS test.

The equivalent shear strain, γ_{eq}, is calculated utilizing Equation 3.12:

$$\gamma_{eq} = \frac{ER}{2} \times V_p \times K_p \times \frac{D}{L} = \frac{0.82}{2} \times V_p \times (0.002805 rad/V) \times \frac{0.0038m}{0.06773m} \times 100\% = 6.45 \times 10^{-5} V_P$$

The area moment of inertia, J_p, is calculated utilizing Equation 3.13:

$$J_p = \frac{\pi D^4}{32} = \frac{\pi (0.038m)^4}{32} = 2.047 \times 10^{-7} \ [m^4]$$

The equivalent shear stress, τ_{eq}, is calculated utilizing Equation 3.14:

$$\tau_{eq} = \frac{ER}{2} \times V_T \times K_T \times \frac{D}{J_p} = \frac{0.82}{2} \times V_T \times (0.1348 \ N \cdot m/rad) \times \frac{(0.038m)}{(2.047 \times 10^{-7} m^4)} = 10.259 V_T \ [kPa]$$

The shear modulus, G, is calculated utilizing Equation 3.15:

$$G = \frac{\tau_{eq}}{\gamma_{eq}} = 159.05 \frac{V_T}{V_P} \ [MPa]$$

After plotting the equivalent stress as a function of the equivalent shear strain, the hysteresis loop is obtained. The hysteresis loop is shown in Figure 7.1.

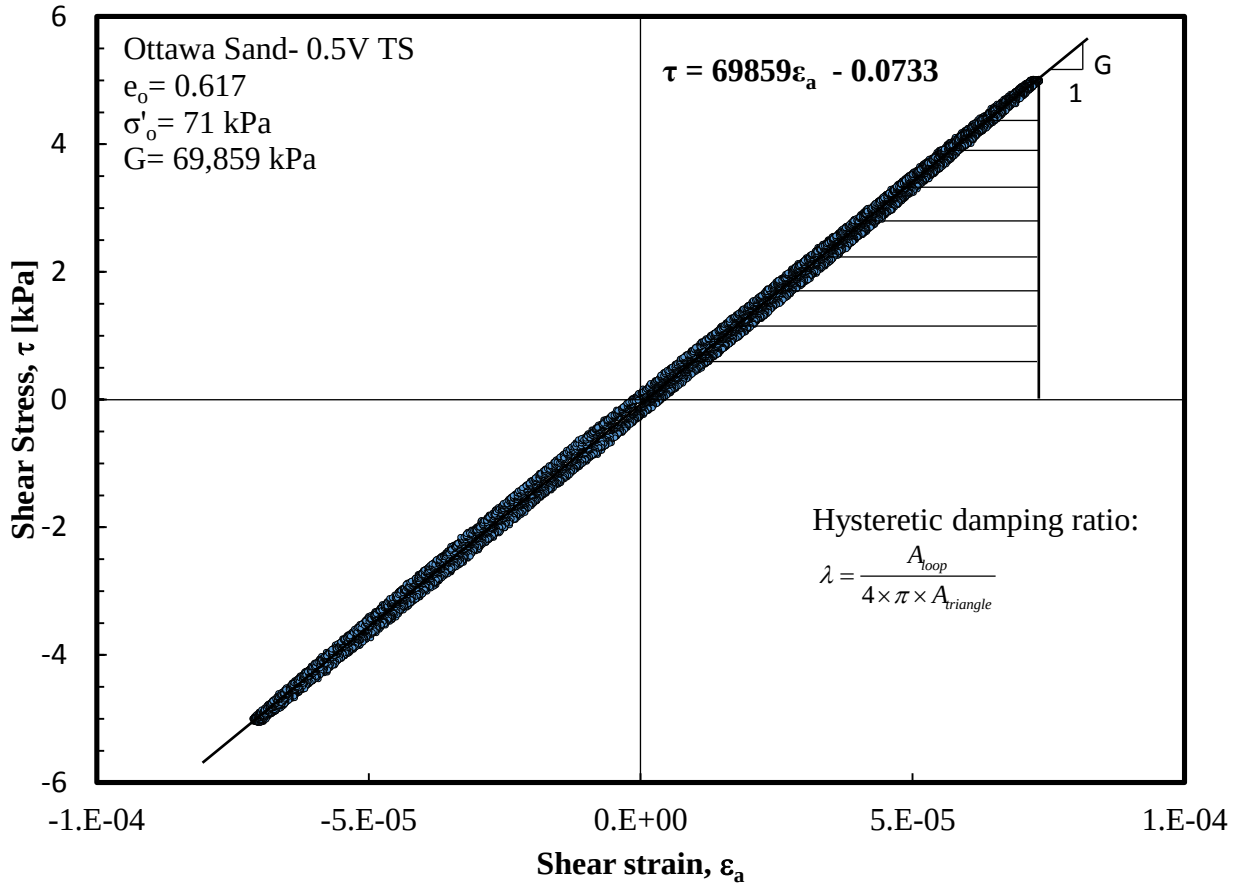

Figure 7.2. Hysteresis loop generated by torsional shear test for Ottawa Sand at 0.5V amplitude.

The shear modulus, G = 69859 kPa= 69.859 [MPa].

The maximum shear strain is: γ_{max}= 7.34x10^{-5}.

The maximum shear stress is: τ_{max}= 5.023 [kPa].

The area of the 1st and 10th cycle loop using MATLAB is: A_{loop}= 3.0514x10^{-5} [kPa].

The area of the crossed triangle is: $A_{triangle}$= (γ_{max} x τ_{max})/2= 1.834x10^{-4} [kPa].

The hysteretic damping ratio, λ, is calculated utilizing Equation 3.16.

$$\lambda = \frac{A_{loop}}{4 \times \pi \times A_{triangle}} = \frac{3.0514 \times 10^{-5}}{4 \times \pi \times 1.834 \times 10^{-4}} \times 100\% = 1.32 \text{ [\%]}$$